PERIODICO di MINERALOGIA
established in 1930

DIPARTIMENTO
DI SCIENZE DELLA TERRA

SAPIENZA
UNIVERSITÀ DI ROMA

An International Journal of
Mineralogy, Crystallography, Geochemistry,
Ore Deposits, Petrology, Volcanology
and applied topics on Environment, Archaeometry and Cultural Heritage

Experimental cannibalization of plagioclase by alkaline basalt magmas

Cristina Perinelli [1,2,*], Alessandro Fabbrizio [3], Barbara Bonechi [4], Mario Gaeta [1], Aida Maria Conte [2]

[1] Department of Earth Sciences, Sapienza University of Rome, P.le Aldo Moro 5, 00185, Rome, Italy
[2] Consiglio Nazionale delle Ricerche, Institute of environmental geology and geoengineering, secondary office of Rome, c/o Department of Earth Sciences, Sapienza University of Rome, P.le Aldo Moro 5, 00185, Rome, Italy
[3] Institute of Petrology and Structural Geology, Faculty of Science, Charles University, Albertov 6, 12843 Prague, Czech Republic
[4] Department of Earth and Environmental Sciences, University of Manchester, Williamson Building, Oxford Road, Manchester M13 9PL, United Kingdom

ARTICLE INFO

Submitted: December 2022
Accepted: January 2023
Available on line: February 2023

* Corresponding author:
cristina.perinelli@uniroma1.it

Doi: 10.13133/2239-1002/17931

How to cite this article:
Perinelli C. et al. (2023)
Period. Mineral. 92, 75-95

ABSTRACT

Time-series crystallization/dissolution experiments were conducted on a natural potassic basalt seeded with bytownitic plagioclases (Plg) at atmospheric pressure, in air, at 1180-1240 °C and isothermal dwell time up to 20 hours. Plg-seed presence promotes the early formation of new-Plg, dampening the clinopyroxene (Cpx) crystallization. New-Plgs grow at a rate from 10^{-6} up to 10^{-8} cm·s^{-1} as the dwell time increases. Seeds overgrow at similar rate. Cpx crystallizes with a delay of at least 3 hours; this has a significant impact on the composition of both residual melt and new-Plgs. For undercooling >35 °C the Cpx delay causes a strong supersaturation of this phase in the melt resulting in a decrease in the new-Plg nucleation rate by 2 orders of magnitude in the 3 h-experiment. In the 15h-run, Cpx coarsening and the decrease of crystallinity suggest the achievement of a near-equilibrium conditions. Cpx growth rate is in the order of 10^{-7} cm·s^{-1} showing very limited variation. Finally, for the investigated superheating (5-15 °C) only the long lasting experiments allows an estimation of Plg dissolution rate (10^{-9} cm·s^{-1}) although changes in the melt composition are already detectable in the 3h-runs.
As a whole our results suggest that in natural systems, the takeover of antecrysts/xenocrysts by a magma can induce on a short time scales, changes in its initial nucleation behavior with remarkable petrological implications for the solidification paths and eruptive dynamics of potassic magmatic systems.

Keywords: crystallization/dissolution experiments; disequilibrium; alkaline magma; heterogeneous nucleation; plagioclase; clinopyroxene.

INTRODUCTION

The texture of a lava points out complex relationships among nucleation and crystal growth. The different textures of lavas with comparable composition indicate the time dependence of transformations during cooling (e.g., Kirkpatrick, 1981; Lofgren, 1983; Cashman, 1990; Dunbar et al., 1995; Higgins, 1998; 2006; Hersum and Marsh, 2006; Hammer, 2008; Mollo and Hammer, 2017). However, the common occurrence of mixed crystal populations of xenocrysts, antecrysts, phenocrysts and microlites in the erupted magmatic products indicate that open-system volcanic processes operated in the volcano

plumbing systems. Against this background, several lines of evidences indicate that magma plumbing systems beneath active volcanoes have developed through a set of crustal reservoirs dominated by relatively liquid-poor crystal mush, i.e., zones made of a semi-rigid framework of crystals within which the melt is distributed (Cashman et al., 2017; Maclennan, 2019). In an open-system volcanic setting, magma intrusions into magmatic mush can rapidly disaggregate and mobilize the cumulate-crystal mush thus accounting for the eruption of distinct crystal populations (Wallace and Bergantz, 2005; Streck, 2008; Kahl et al., 2011; Huber et al., 2012; Thomson and Maclennan, 2013; Bergantz et al., 2015) some of which out of equilibrium with their carrier liquids (Passmore et al., 2012; Neave et al., 2013; Moore et al., 2014).

Many experimental studies focused on the kinetic effects of crystallization of magmas and how they profoundly affects the physico-chemical properties of such melts and the morphology and composition of the mineral formed by the magma (e.g., Lofgren et al., 1974; Donaldson, 1976; Kirkpatrick, 1981; Hammer and Rutherford, 2002; Couch et al., 2003; Zieg and Lofgren, 2006; Hammer, 2008; Pupier et al., 2008; Del Gaudio et al., 2010; Iezzi et al., 2011; Mollo et al., 2011, 2012a, 2013; Iezzi et al., 2014; Arzilli et al., 2015; Waters et al., 2015; Bonechi et al., 2020 a,b; Giuliani et al., 2020; Masotta et al., 2020; Bonechi et al., 2021a; Arzilli et al., 2022; Di Fiore et al., 2022). Some of these have also explored the crystal nucleation and growth processes in systems formed by a glass-mineral mixture (e.g., Lofgren, 1983; Couch, 2003; Larsen, 2005; Orlando et al., 2008; Shea and Hammer, 2010; Mollo et al., 2012b; Bonechi, 2020). Among the latter, however, only few studies involve the dissolution of pre-existing crystals (e.g., Tsuchiyama and Takahashi, 1983; Kuo and Kirkpatrick, 1985 a,b; Van Orman and Grove, 2000; Liang, 2003; Zieg and Lofgren, 2006; Agostini et al., 2013; Bonechi, 2020; Bonechi et al., 2021b) although the dissolution is an important process in petrogenesis of igneous rocks (e.g., magma genesis by partial melting, assimilation of xenoliths, partial to total resorption of minerals during magma mixing; Brearley and Scarfe, 1986; Tsuchiyama, 1986, Liang, 2003; Morgan and Liang, 2003; Tursack and Liang, 2012).

To provide a contribution on the understanding of the kinetics of a process such as the recharge of fresh magma driving the magmatic system towards new physical and chemical equilibrium conditions, we carried out time-series crystallization/dissolution experiments on a potassic basalt, namely PST-9 *golden* pumice from Stromboli volcano (Aeolian arc, southern Italy), at atmospheric pressure and in a range of temperature between 1180 °C and 1240 °C. The chosen thermal conditions bracket the liquidus temperature of the potassic basalt (~1225 °C at P=0.1 MPa) i.e., the lowest temperature of minerals dissolution and the highest temperature at which crystals start to grow. We focused on plagioclase because, among the most abundant minerals in basic volcanic rocks, it is stable under a wide range of physico-chemical conditions and sensitive to changes in thermodynamic parameters during its growth in magma storage and transport zones (e.g., Lofgren, 1980; Tsuchiyama and Takahashi, 1983; Nelson and Montana, 1992; Johannes et al., 1994; Viccaro et al., 2010). But chiefly because the complex textures of the PST9-plagioclases reflect the chemical disequilibrium between this phase and the host melt indicating the remobilization of a shallow resident magma and that these crystals were incorporated into the pumice during the eruption (Pichavant et al., 2011)

EXPERIMENTS

Table 1 lists the notations used in this paper.

Table 1. Notations used in the paper.

	notation	range investigated
Area fraction of microlites determined by image analyses	ϕ	
Clinopyroxene newly microlites	Cpx	
Disequilibrium degree of plagioclase	ΔAn	
Dissolution rate of plagioclase seed	*D*	
Experimental time elapsed at isothermal conditions	t	0-20 h
Growth rate	*G*	
Maximum length of crystals	L	
Nucleation rate	*J*	
Oxide	Ox	
Plagioclase Tiger Gabbro seed	PlgTG	
Plagioclase overgrown rim	PlgS	
Plagioclase newly microlites	PlgN	
Standard deviation	σ	
Temperature	T	1180-1240 °C
Undercooling (+)/ overheating (-) value	ΔT	

Starting materials and experimental procedures

Growth and dissolution experiments were conducted using as starting material a potassic basalt (*golden* pumice sample PST-9; Pichavant et al., 2011) erupted in the period AD 800-1600 (Table 2). PST9 sample is glassy, strongly vesicular (60 vol.% vesicles) and phenocryst poor (~11 vol.% crystals) with clinopyroxene and subordinate olivine and plagioclase (see Pichavant et al., 2011 for details). Plagioclase seeds were hand-picked from a gabbro rock belonging to the layered ultramafic intrusive complex of Tiger Gabbro (northern Victoria Land, Antarctica Ganovex Team, 1987). The seeds are homogeneous and have compositions (An_{76-78}; Table 2) within the range of those of PST9 plagioclases identified in literature as xenocrysts (An_{70-88}; Pichavant et al., 2011 and references therein). To minimize possible differences in growth rates due to the different crystallographic directions, seeds with tabular habit, ranging in size between 500 and 700 mm on each side, and with low aspect ratio (Larsen, 2005) were selected.

The experiments were performed in the laboratory of the Dipartimento di Scienze della Terra at the University of Camerino. They were run in air, in a Deltech vertical furnace (model DT-31VT-OS2) equipped with 2B controlling thermocouple and an additional S monitoring thermocouple. The experimental temperatures ranged from 1180 °C to 1240 °C (at 0.1 MPa). In each runs a seed of plagioclase was added to PST-9 powder in a ratio plagioclase seed:PST9 powder of ~0.03:1. In order to remove any crystals from PST-9 natural powder, this latter was previously melted at 1300 °C for 3 hours. The homogeneity of the glass was checked by optical observations and EMP analyses. No loss of Fe and alkali has been revealed.

A platinum box containing the rock-crystal assemblage was suspended with a platinum wire next to the monitoring thermocouple at the hot spot of the furnaces. The experiments were carried out starting from the temperature previously determined (i.e., 1225 °C), at which no crystallization or dissolution process is detectable at the plagioclase seed-melt interface at micrometric scale of our analyses (Figure S1 in Supplementary materials). Charges were held for 2 minutes at these conditions and then the temperature was dropped/ramped up to the experimental T with a linear cooling gradient of 100 °C/h. For each investigated T, dwell time was in the range of 0-20 hours (Table 3).

Table 2. Starting material composition.

	PST9[a]	PlgTG[b]	
	Bulk		σ
SiO_2	50.49	48.82	0.64
TiO_2	0.86	0.02	0.01
Al_2O_3	15.38	32.17	0.31
FeO_t	7.62	0.33	0.10
MnO	0.21	-	-
MgO	7.69	0.05	0.02
CaO	12.48	15.65	0.53
Na_2O	2.32	2.42	0.16
K_2O	1.88	0.12	0.15
P_2O_5	0.47	-	-
L.O.I.	0.45	-	-
Total	99.85	99.56	
An mol%		77.05	1.71

a: Bulk composition of Stromboli *golden* pumice after (Conte et al., 2006); FeO_t = total Fe as FeO. b: Tiger Gabbro plagioclase used as seed crystals; An = anorthite component of plagioclase; L.O.I. = loss on ignition.

Table 3. Experimental conditions and phases assemblage in run products.

Run	T (°C)	ΔT (°C)	t (h)	Phase
C1	1180	45	0	Gl, Ox , PlgS, PlgN
C2	1180	45	3	Gl, Ox , PlgS, PlgN, Cpx
C3	1180	45	15	Gl, Ox , PlgS, PlgN, Cpx
C4	1190	35	0	Gl, Ox , PlgS, PlgN
C5	1190	35	3	Gl, Ox , PlgS, PlgN, Cpx
C6	1190	35	15	Gl, Ox , PlgS, PlgN, Cpx
C7	1200	25	0	Gl, Ox , PlgS, PlgN
C8	1200	25	3	Gl, Ox , PlgS, PlgN
C9	1200	25	15	Gl, Ox , PlgS, PlgN, Cpx
C11	1220	5	3	Gl, Ox , PlgS, PlgN
C12	1220	5	10	Gl, Ox , PlgS, PlgN
C13	1220	5	20	Gl, Ox
D1	1230	-5	3	Gl, Ox
D2	1230	-5	10	Gl, Ox
D3	1230	-5	20	Gl, Ox
D4	1240	-15	3	Gl
D5	1240	-15	10	Gl
D6	1240	-15	20	Gl

ΔT: $T_{liquidus}$-$T_{experiment}$, undercooling (+)/overheating (-) value; t: time elapsed at isothermal conditions; Gl: glass; Ox: oxides; PlgS: plagioclase overgrown rim; PlgN: newly plagioclases; Cpx: clinopyroxene microlites.

At the end of the experiment the charge was quenched in deionized ice water.

ANALYTICAL TECHNIQUES

Texture and composition

Texture relationships of each run were examined by electronic back-scattered (BSE) images collected at the Dipartimento di Scienze della Terra of Sapienza, University of Rome, using a Philips XL30 SEM. The scanning beam conditions used for imaging were 20-keV accelerating voltage and a 30 nA. The EDS multi-element chemical maps (1024x768 pixel mapping resolution) were collected at the CNR -Montelibretti laboratory, using a ZEISS EVO MA10 scanning electron microscope, equipped with EDS Oxford microanalysis. Operating conditions were: EHT 20 KeV, working distance 8.5 mm and I Probe current of 50 pA.

Microanalyses of phases composition were performed on polished carbon-coated mounts by a 4-spectrometer Cameca SX50-52 electron microprobe with PAP correction procedures for all phases, using a 15-keV accelerating voltage and a 15 nA beam current (at CNR-IGAG, Rome). The standards employed were: metals for Mn and Cr, jadeite for Na, wollastonite for Si and Ca, orthoclase for K, corundum for Al, magnetite for Fe, rutile for Ti, periclase for Mg, apatite for P. For all elements the counting times were 20 s on peak and 10 s on both backgrounds. Light elements (Na, K) were counted first to prevent loss by volatilization. A focused beam was used for minerals, while glasses were analyzed with a 10 μm diameter beam to minimize volatilization of sodium. The accuracy of the analyses was evaluated by repeated analyses of three international secondary standards (Kakanui augite, Iceladic Bir-1 and rhyolite RLS132 glasses from USGS) made prior to any series of measurements. The mean precision from the standard value was about 1% for SiO_2, 2% for Al_2O_3, 5% for K_2O, CaO and FeO, and 8-10% for other elements. The analytical precision (2 sigma error) is 1% for elements in the concentration range >10 wt% oxide, 5% for elements in the range 2-10 wt% oxide and better than 10% for elements in the range 0.5-2 wt% oxide.

Image analysis

Six to ten backscatter electron images at different scale were collected for each experimental sample. In the growth runs, the newly grown rim is easily recognized from the images for its clearer shade of grey with respect to that of the seed (Figure 1) and about 10 measures of the new rim were collected along two edges for each crystal. Average rim growth rates (G_{PlgS}) were calculated by dividing the average of the widths by the total experimental run time (Larsen, 2005). The lengths

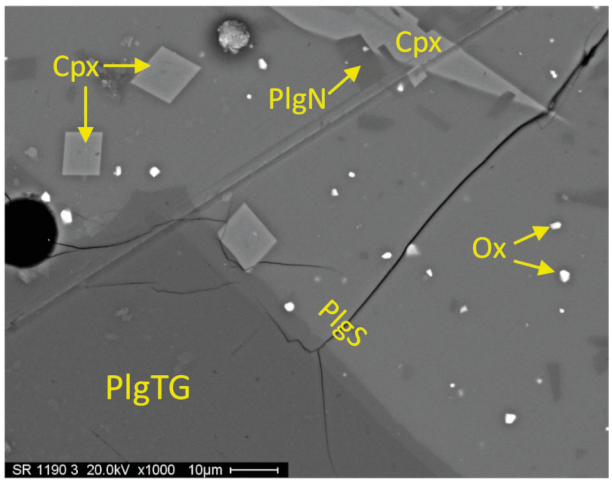

Figure 1. Representative back-scattered electron (BSE) image from experiment C5 (1190 °C - 3h dwell time). The new rims grown around plagioclase seed (PlgTG) recognizable for their different grey shade (dark and light grey for seed and new rim, PlgS, respectively). Plagioclase (PlgN) and clinopyroxene (Cpx) and oxides (Ox) microcrystals crystallized in the groundmass are also visible in the image.

(l) and widths (w) of plagioclase and clinopyroxene microlites crystallized were obtained from 3-4 images of each experiment. The growth rates of plagioclase (G_{PlgN}) and clinopyroxene (G_{Cpx}) microlites were determined using the method reported by Larsen (2005) dividing the average equivalent spherical ratio [$r_{eq}=(l*w/\pi)^{1/2}$] of the 10 largest microlites by the experimental duration. The images were subsequently processed and analyzed using ImageJ software (http://rsb.info.nih.gov/ij/) to obtain the area fractions (ϕ) of plagioclase and clinopyroxene microlites. The volumetric number densities (N_v) of microlites were evaluated as in Larsen (2005) computing from each image the number of crystals per unit area (N_a) and evaluating the characteristic crystal size ($S_n=\phi/N_a)^{1/2}$, with $(N_v)=N_a/S_n$. The minimum nucleation rates (J) were obtained by dividing the N_v by the total experimental duration.

In the experiments at T>1225 °C the widths of crystals dissolved were difficult to determine and only for the longest runs was possible to estimate the dissolution rate (D) which was calculated by measuring the height of the roughness (cuspate and pillars, see section § "*Results*") of the crystal rim and dividing the average of collected measures (at least 4 for each run) by the experimental duration.

RESULTS

The results of our experiments are shown in Table 3. Overall, the plagioclase seed (PlgTG) is reabsorbed at

T>1225 °C whereas at lower temperatures it always shows a visible overgrown rim (PlgS) although in the longest experiment at 1220 °C it is almost completely reabsorbed (Figure 2). Starting from 1220 °C plagioclase also occurs as microlites (PlgN), that at this temperature appear as rare micrometric (<10 μm) tabular crystals. Except for the runs at 1240 °C, all experimental charges contain oxide crystals (Table 3), confirming their oxidized nature. Instead, the first occurrence of clinopyroxene (Cpx) is at 1200 °C.

Growth/dissolution experiments: textural and compositional evolution of plagioclase seed

Table 4 summarizes the key data on texture and phase abundances.

Crystallization experiments

Plagioclase seeds are reabsorbed at T>1225 °C whereas at lower temperatures they present always a visible overgrown rim. At T=1220 °C rare micrometric plagioclases crystallize after 3 hours while a thin overgrown rim covers the seeds at all isothermal rest time, increasing in size up to ~1.1 μm in the C12 (dwell time 10h). However, in this experiment the overgrown rim shows incipient resorption features in the form of regularly embayed boundaries, subhedral grain boundary segments, as well as rounded corners (Figure 2b). Such dissolution features become clearly apparent in the 20h rest time run in which the new rim is reduced up to ~0.3 μm (Figure 2c). However, it should be said that this precipitation-dissolution process could be due to small temperature fluctuations unavoidable in experiments of long durations (Simakin and Bindeman, 2008).

At lower temperatures the thick of the rims ranges from 1 to ~10 μm with the widest overgrowth measured in the longest experiment at 1190 °C. The morphologies of the new rims are in general regular in shape with sharp contacts although in the shortest experiments they display discontinuities and lumps (Figure S2 in Supplementary materials). In all cases the rim growing around the top edge of the seed is wider than that growing along the vertical edge, indicating a crystallographic control on growth rate.

A first-order of evidences is shown by the influence of temperature and dwell time on growth rate (G_{PlgS}) at isothermal conditions. The mean rim width developed during the cooling to the temperature of interest (0-h runs) results in a similar G_{PlgS} (~$1 \cdot 10^{-6}$ cm·s^{-1}) for ΔT of 25 °C and 35 °C and in a lower G_{PlgS} (~$1 \cdot 10^{-7}$ cm·s^{-1}) for a ΔT=45 °C (Table 4 and Figure 3a). This behavior is also evident in the runs with the final isothermal plateau although the differences in G_{PlgS} are smoothed as the experimental timescale is increased (Figure 3a). The stall

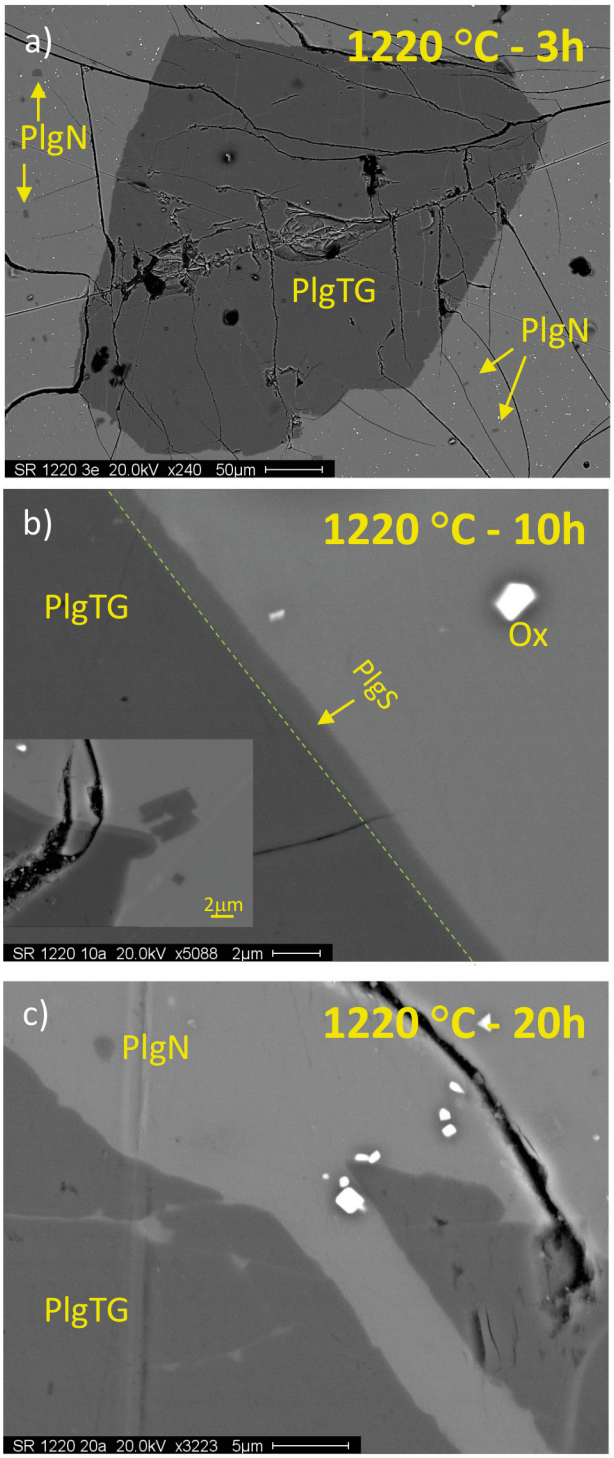

Figure 2. BSE images of time-series experiments at 1220 °C. a) Beside the oxides microcrystals newly tabular plagioclases (PlgN) are visible dispersed in the experimental glass. b) C12 and c) C13 time-series experiments (10h and 20h dwell time, respectively) during which the overgrown rim on PlgTG resorbs as the isothermal rest time increases. Dashed green line outlines the seed-PlgS transition.

Table 4. Textural parameters and estimated nucleation and growth rates.

				Plagioclase									*Clinopyroxene*			*Oxide*
Run	T (°C)	ΔT (°C)	t (h)	G_{PlgS} (cm s^{-1})	σ	D (cm s^{-1})	G_{PlgN} (cm s^{-1})	σ	J_{PlgN} (cm^{-3} s^{-1})	L (cm)	Aspect ratio PlgN	ϕ_{PlgN} (%)	G_{Cpx} (cm s^{-1})	σ	ϕ_{Cpx} (%)	ϕ_{Ox} (%)
C1	1180	45	0	$4.0 \cdot 10^{-7}$	$3 \cdot 10^{-8}$		$1.7 \cdot 10^{-6}$	$3 \cdot 10^{-7}$	$1.2 \cdot 10^{3}$	$1.4 \cdot 10^{-3}$	1.64	1.0				0.6
C2	1180	45	3	$3.1 \cdot 10^{-8}$	$7 \cdot 10^{-9}$		$7.3 \cdot 10^{-8}$	$3 \cdot 10^{-9}$	$1.8 \cdot 10^{2}$	$2.9 \cdot 10^{-3}$	2.27	1.8	$9.9 \cdot 10^{-8}$	$4 \cdot 10^{-9}$	21.4	3.8
C3	1180	45	15	$7.8 \cdot 10^{-9}$	$6 \cdot 10^{-10}$		$1.6 \cdot 10^{-8}$	$6 \cdot 10^{-9}$	$9.6 \cdot 10^{1}$	$3.8 \cdot 10^{-3}$	2.46	7.9	$8.8 \cdot 10^{-8}$	$6 \cdot 10^{-9}$	13.1	1.7
C4	1190	35	0	$1.2 \cdot 10^{-6}$	$4 \cdot 10^{-7}$		$2.8 \cdot 10^{-6}$	$6 \cdot 10^{-7}$	$7.9 \cdot 10^{5}$	$1.7 \cdot 10^{-3}$	1.36	3.0				0.4
C5	1190	35	3	$5.0 \cdot 10^{-8}$	$8 \cdot 10^{-9}$		$1.1 \cdot 10^{-7}$	$1 \cdot 10^{-8}$	$1.2 \cdot 10^{3}$	$2.8 \cdot 10^{-3}$	1.93	8.3	$2.0 \cdot 10^{-7}$	$4 \cdot 10^{-8}$	8.3	0.5
C6	1190	35	15	$1.5 \cdot 10^{-8}$	$1 \cdot 10^{-9}$		$2.7 \cdot 10^{-8}$	$4 \cdot 10^{-9}$	$2.9 \cdot 10^{2}$	$3.6 \cdot 10^{-3}$	1.51	12.2	$7.4 \cdot 10^{-8}$	$7 \cdot 10^{-9}$	14.3	0.6
C7	1200	25	0	$9.4 \cdot 10^{-7}$	$2 \cdot 10^{-8}$		$3.1 \cdot 10^{-6}$	$2 \cdot 10^{-7}$	$3.1 \cdot 10^{5}$	$1.6 \cdot 10^{-3}$	1.82	0.9				0.5
C8	1200	25	3	$3.4 \cdot 10^{-8}$	$4 \cdot 10^{-9}$		$9.9 \cdot 10^{-8}$	$1 \cdot 10^{-8}$	$1.6 \cdot 10^{3}$	$1.8 \cdot 10^{-3}$	2.07	3.4				0.5
C9	1200	25	15	$9.5 \cdot 10^{-9}$	$1 \cdot 10^{-9}$		$2.2 \cdot 10^{-8}$	$2 \cdot 10^{-9}$	$1.7 \cdot 10^{2}$	$3.0 \cdot 10^{-3}$	1.92	2.4	$8.4 \cdot 10^{-8}$	$7 \cdot 10^{-9}$	n.d.	0.5
C11	1220	5	3	$2.3 \cdot 10^{-9}$	$4 \cdot 10^{-10}$		n.d.					trace				0.1
C12	1220	5	10	*$3.1 \cdot 10^{-9}$*	*$2 \cdot 10^{-10}$*		n.d.					0.3				0.1
C13	1220	5	20	*$1.7 \cdot 10^{-9}$*	*$1 \cdot 10^{-10}$*		n.d.									0.2
D1	1230	-5	3	n.d.												
D2	1230	-5	10			$4.6 \cdot 10^{-9}$										
D3	1230	-5	20			$4.5 \cdot 10^{-9}$										
D4	1240	-15	3			n.d.										
D5	1240	-15	10			n.d.										
D6	1240	-15	20			$1.5 \cdot 10^{-9}$										

Notes: $\Delta T = T_{liquidus} - T_{experiment}$, undercooling (+)/overheating (-) value; G= growth rate; D=dissolution rate; J= nucleation rate; L= maximum length; PlgS=plagioclase overgrown rim; PlgN= plagioclase microcrysts; Cpx= clinopyroxene microcrysts; Ox= oxides. ϕ = microcrystals area fraction determined by image analyses; G_{PlgS} values in italic are the net growth rate that results from a balance of growth and the resorption of rim overgrown on the plagioclase seed (see the text).

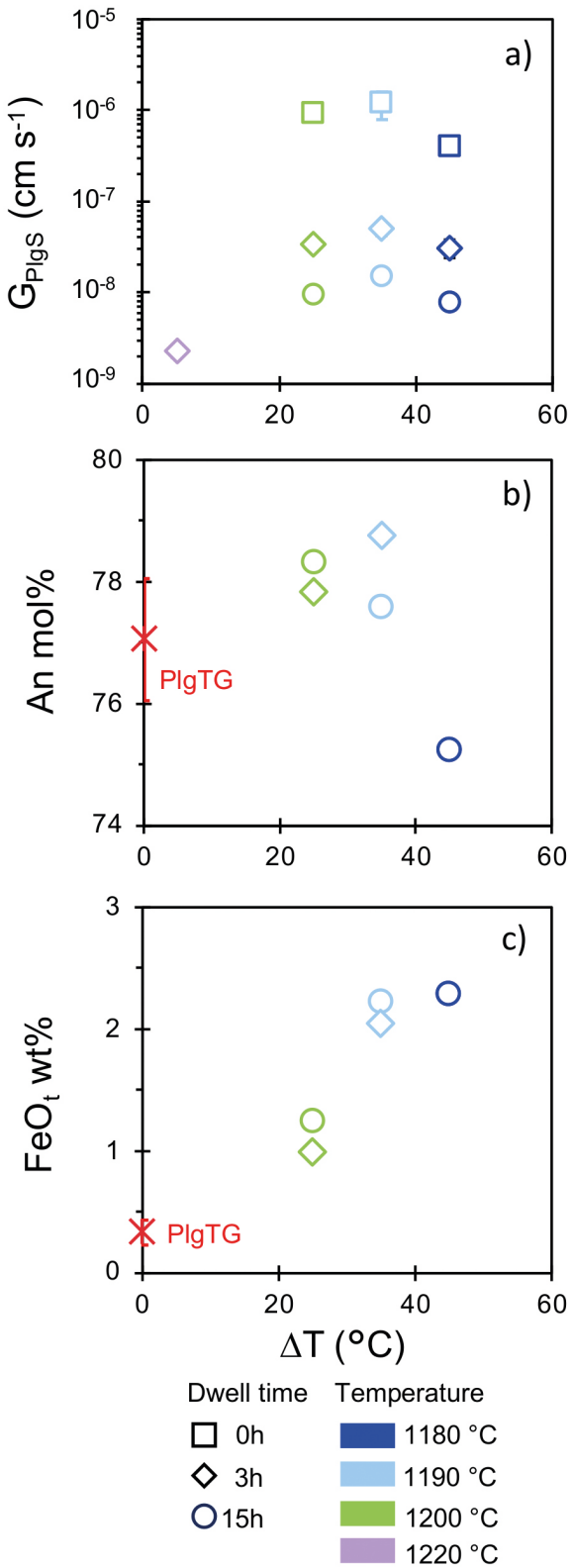

Figure 3. Variation of a) estimated growth rate b) anorthite and c) FeO_t contents of plagioclase overgrowth rim as function of undercooling degree.

on isothermal conditions produces significant variations on G_{PlgS} at $\Delta T \geq 25$ °C that decreases of about 2 order of magnitude (G_{PlgS} ~$1 \cdot 10^{-8}$ cm·s^{-1}) after 3 hours (3-h runs) of dwelling. Increasing the time elapsed at the final isothermal plateau, 15-h runs, G_{PlgS} still decreases but the variations with respect to that calculated from 3-h runs, are low (about half order of magnitude, Table 4). At small ΔT (ΔT=5 °C) G_{PlgS} is ~$2 \cdot 10^{-9}$ cm·s^{-1} for the short dwell time experiment (C11-3h run), similar to the value estimated for the C12 experiment (10h dwell time, G_{PlgS}=$3.1 \cdot 10^{-9}$ cm·s^{-1}; Table 4). However, it should be emphasized that, albeit in a limited way, the latter value represents the net growth rate resulting from a balance of growth and the incipient resorption of the PlgS (see above). Similarly, the net growth rate calculated for C13 experiment (20h dwell time) is in the order of 10^{-9} cm·s^{-1}.

The composition of the overgrown rims has been determined only for the runs that have PlgS wide enough for accurate analyses (Table S1 in Supplementary materials). It was measured along two edges of each crystal so as to take into account the random crystallographic orientation in determining the average composition. Concerning the anorthite component, the composition of the overgrown rims does not deviate significantly from that of the seeds and is scarcely affected by the increase in ΔT ($T_{1225°C}$-T_{run}) showing only a slight decrease from An_{78} to An_{75} (Figure 3b). Conversely, overgrown rims are well distinguished from the seeds for their higher FeO_t content (0.3 wt% and >0.9 wt%, respectively), which increases from 0.94 wt% to 2.28 wt% increasing the DT (Figure 3c). Such FeO_t increase reflects the positive correlation of the silica content of a magma with the partitioning of ferric iron ($DFe_2O_3^{Plg\text{-}liq}$; Lundgard and Tegner, 2004) that we have to take into account due to the oxygen fugacity imposed for the experiments that make the iron in the melt almost all as Fe_2O_3. Actually, the $\Delta Fe_2O_3^{Plg\text{-}liq}$ is estimated to be up to 0.9 for alkaline melts with a SiO_2 content similar to that of the residual glasses obtained at 1180 °C (C2 and C3 runs SiO_2=54-55 wt%).

Dissolution experiments

Plagioclase seed at T>1225 °C was not stable reacting to dissolve. Dissolution produced generally sharp PlgTG-glass interface, rounded smoothed crystal edges and small waves with amplitude of 10-20 μm along the crystal rims (Figure 4a). PlgTG of the experiments at 1230 °C (D2 and D3) and 1240 °C (D5 and D6) is characterized by rough contacts with the glass, represented by cusps and pillars standing 5-10 μm above the receding rims. Micrometric anhedral to rounded crystals are suspended above the dissolution horizon (Figure 4b). Similar dissolution features are described by Laumonier et al. (2019) who experimentally studied the dissolution and precipitation

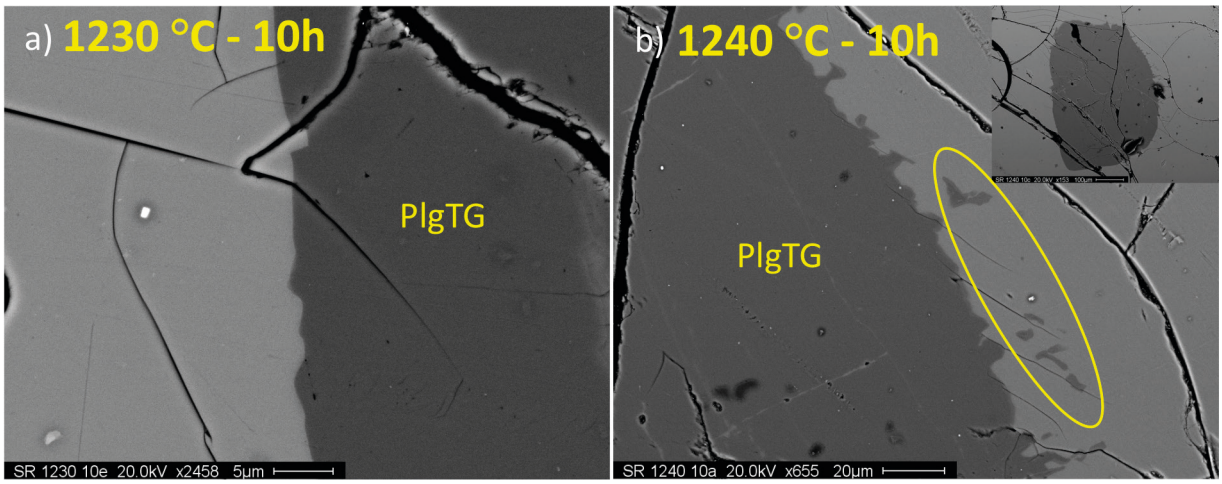

Figure 4. Back-scattered electron images showing dissolution the features of plagioclase seed produced by dissolution experiments a) D2 (1230 °C and 10 h) and b) D5 (1240 °C and 10 h). In b) small pieces are visible that have detached from the PlgTG.

process of forsteritic olivines in a haplobasaltic composition under thermal gradient conditions.

Locally glass-filled channels enter the crystal following cracks that in several cases produce complete necking and isolation of small pieces of PlgTG.

Slight changes in composition of residual PlgTG are observed only in the longest experiment at 1240 °C (D6-20h) which shows a minimal decrease of Al_2O_3 and an increase in FeO_t content from ~0.33 wt% to ~0.94 wt% at its margin (Table S1 in Supplementary materials).

The estimation of dissolution rate is difficult due to the geometry of the charges that does not allow to avoid convection during the experiments. However, because in convective conditions the dissolution rate does not depend on the crystallographic orientation but scales with dwell time (e.g., Brearley and Scarfe, 1986; Donaldson, 1985; Kuo and Kirkpatrick, 1985b), an approximate estimation of the dissolution rate (D) of pristine plagioclase is given here for the longest dissolution experiments whose peculiar dissolution textures allow for a rough estimate of the amount of the crystal margin receded. Taking the above into account, D calculated for experiments show no significant differences being all in the order of D~$1 \cdot 10^{-9}$ $cm \cdot s^{-1}$ (D=$4.6 \cdot 10^{-9}$ $cm \cdot s^{-1}$ in D2 run; D=$4.5 \cdot 10^{-9}$ $cm \cdot s^{-1}$ in D3 run; D=$1.5 \cdot 10^{-9}$ $cm \cdot s^{-1}$ in D6 run; Table 4).

Newly crystals distribution

Oxide is a ubiquitous phase except for the runs at 1240 °C. It is present as tiny (≤5 μm) polygonal crystals dispersed in the matrix, often too small for reliable electron microprobe analysis. The few analyses collected reveal that they are magnetites with the ulvospinel component in the range between 2.5 and 3.5 mol% (Table S1 in Supplementary materials). Oxide microlites crystallization seems to be independent from run time (Table 4).

Plagioclase crystals developed in all the runs characterized by undercooling. At 1220 °C they are rare and appear as micrometric (<10 μm) tabular crystals located in an area at a distance ≤150 μm from the seed boundary in the shortest experiment (Figure 2a). In longer-term experiments, such as PlgS, the PlgN sometimes show blunt corners (Figure 2c).

At 1200 °C clinopyroxenes join PlgN only in the longest experiment (C9-15h) in which Cpx show a tabular habit and occasionally they include 1-20 μm long tabular PlgN. Then Cpx is always present except for runs in which the duration time is 0 hours (Table 3) indicating that this phase does not form during the experimental cooling step.

Decreasing temperatures PlgN with skeletal and acicular habits (<20 μm in size) occur along with tabular microcrysts in the shortest experiments (0 time runs). In the other rest-time experiments PlgN have tabular morphologies and reach a maximum size of ~40 μm (Table 4).

Prismatic to tabular Cpx, present in both 1190 and 1180 °C, t>0h experiments, reach size greater than 100 μm in the long lasting experiments (15 hours, C3-C6 runs) where they even form intergrowths (i.e., monomineralic glomerocrysts; Figure 5). The largest crystals occasionally exhibit normal or sector zoning while commonly entrap several small plagioclase microlites.

As regards the growth rate of PlgN as a function of undercooling it can be observed that as a general rule it slightly decreases as the undercooling degree increases (Figure 6a). Considering the experiments performed at the same temperature, it is evident that the growth rates

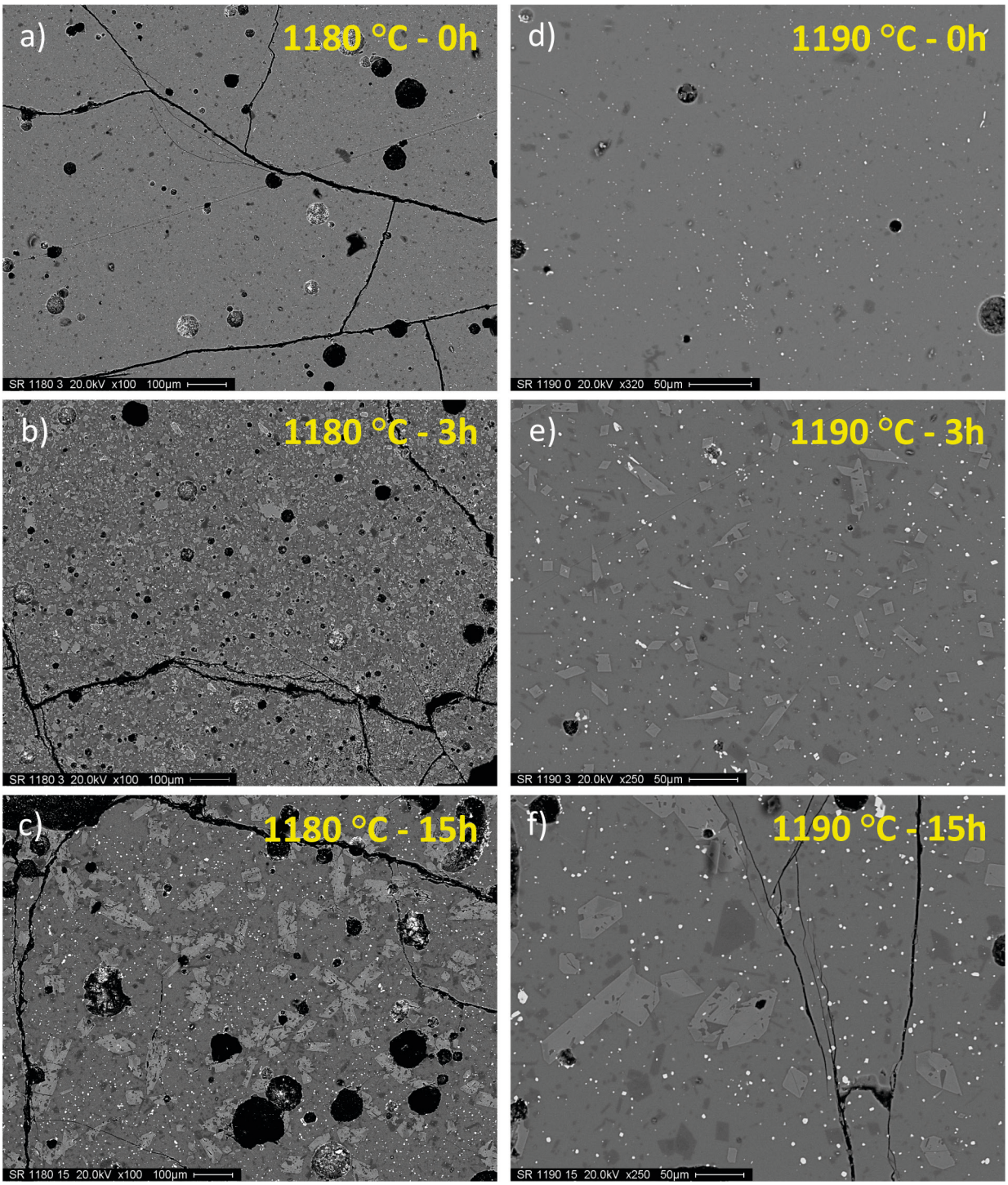

Figure 5. Representative BSE images of products of 1180 °C and 1190 °C time-series experiments. Images show the evolution of textures as a function of experimental duration. Dark grey are plagioclases, high-contrast phases are Fe-Ti oxides and light grey crystals are clinopyroxenes.

of plagioclase crystals decrease exponentially with the experimental time: crystals formed during the cooling step of experiments (i.e., 0 hours rest time runs - C1, C4 and C7) grow at a rate of the order of 10^{-6} cm·sec^{-1}, while the growth rate estimated for the isothermal rest-time experiments of 3 and 15 hours drops by one (G_{PlgN}

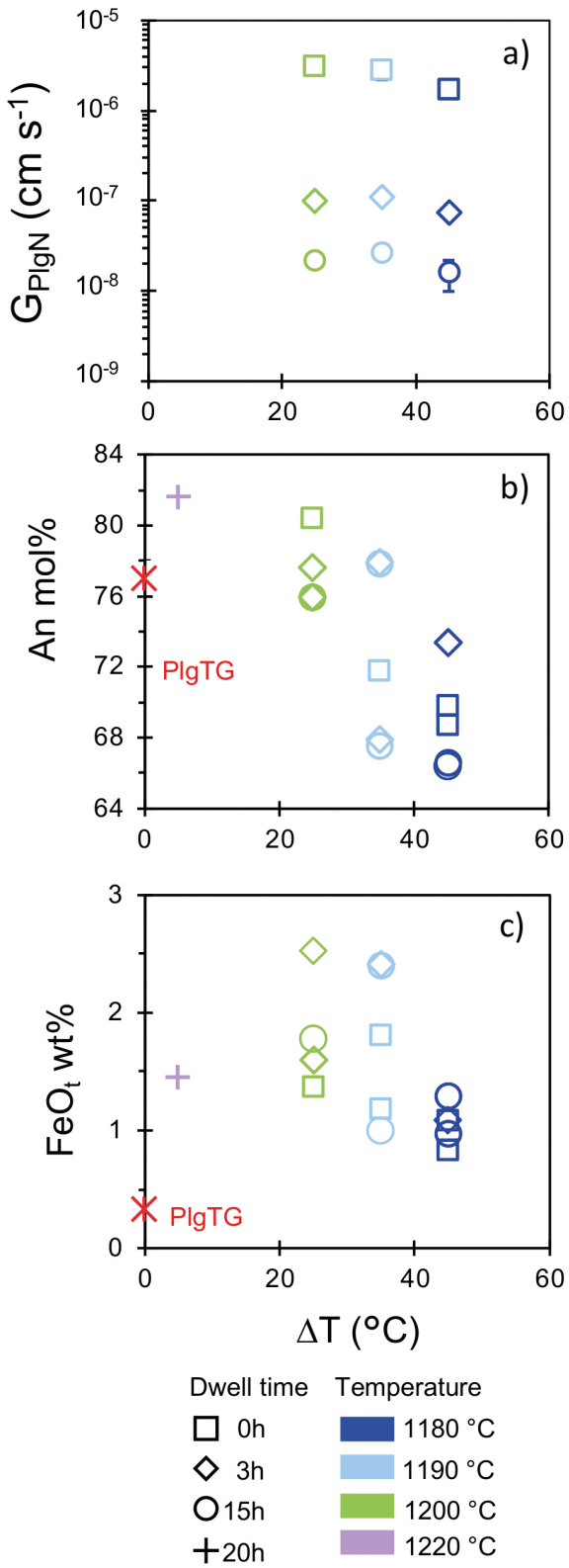

Figure 6. Variation of a) estimated growth rate b) anorthite and c) FeO_t contents of plagioclase newly crystals as function of undercooling degree.

~$1 \cdot 10^{-7}$ cm·s^{-1}) and two (G_{PlgN} ~$2 \cdot 10^{-8}$ cm·s^{-1}) orders of magnitude respectively (Figure 6).

Moreover, for the isothermal experiments the maximum length of microcrystals increases linearly with experimental time and for runs of the same duration is higher at lower temperature. The nucleation rates vary between $2 \cdot 10^{2}$ and $8 \cdot 10^{5}$ cm^{-3}·s^{-1} decreasing exponentially with runs duration (Table 4).

Concerning clinopyroxenes, the estimated growth rate values show limited variability at around $1 \cdot 10^{-7}$ cm·s^{-1} seeming it almost to be independent with respect to the investigated ΔT and the experimental time.

Newly crystals composition

PlgN composition varies between An_{82-66} within the range of natural crystals in PST9 (An_{81-63}). Overall, the anorthite content decreases with decreasing temperature although in the rest-time experiments PlgN with different compositions coexist as in the C5 and C6 runs (i.e., 1190 °C - 3h and 15h; Figure 6b) where high An (78 mol%) and low An (68 mol%) both occur. Notably, some PlgN crystals are zoned (Figure 5f) however, it was not possible to obtain accurate analyses of the cores due to their small size. Finally, as observed for the PlgS, high contents of FeO_t characterized all PlgN (Figure 6c).

Clinopyroxene has augitic composition in all the experiments. Limited compositional changes are observed between the 3h and 15h runs at 1190 °C contrary to what detected from 3h and 15h runs at 1180 °C in which Cpx from C2-3h run have higher SiO_2 (49-52 wt%) and lower TiO_2 (~0.7 wt%), Al_2O_3 (2.7-3.9 wt%), and FeO_t (~8 wt%) than those of clinopyroxenes in C3-15h run (SiO_2 ~46 wt%, TiO_2 ~0.85 wt%, Al_2O_3 ~7 wt%, and FeO_t ~9 wt%; Table S1 in Supplementary materials).

Compositional variations in glasses

The compositions of the experimental glasses are reported in Table S1 (in Supplementary materials) and shown in the Total Alkali versus Silica (TAS) classification diagram (Le Maître et al., 2002) and in a time vs oxides plot (Figure 7). The most significant changes in melt composition due to crystallization are observed in the experiments at ΔT>25 °C and isothermal dwell time >0h which produced basaltic-andesite to basaltic trachyandesite (Figure 7a). Synthetic glasses produced at temperatures of 1200-1220 °C have chemistry close to the starting material one regardless of the experimental time, although the residual glass at 1200 °C shows a marginal depletion of CaO and Al_2O_3 content due to the incoming plagioclase crystallization. The glasses of the experiments at lower temperatures (1180-1190 °C) show a marked increase in SiO_2, Na_2O, K_2O and TiO_2, coupled with a decrease of CaO, MgO and FeO contents reaching their

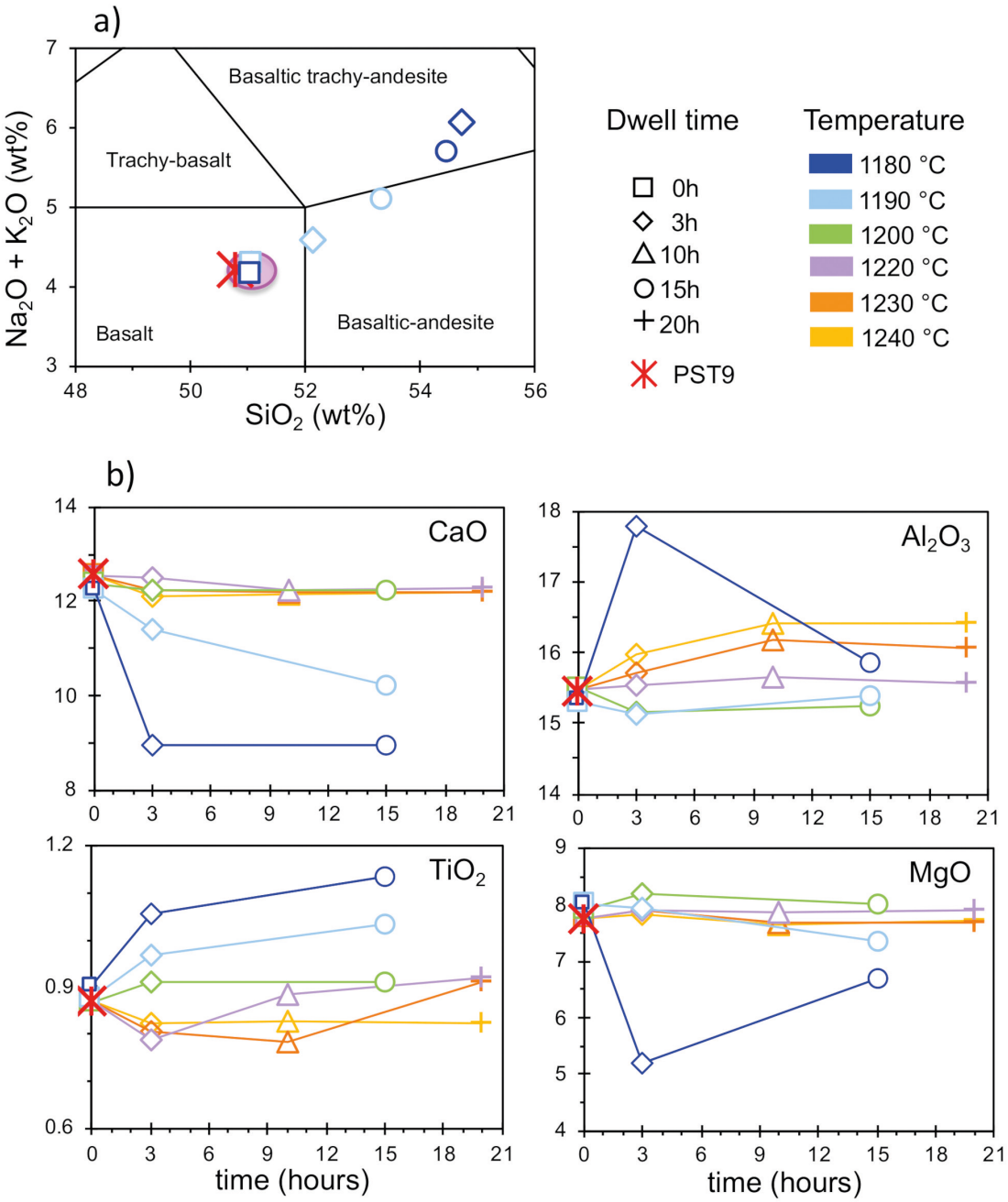

Figure 7. a) Total alkali versus silica classification diagram (TAS, Le Maitre et al., 2002) and b) dwell time versus selected oxides plots for experimental glasses. Pink field in the TAS plot includes the compositional variation of glasses from time-series experiments at 1220-1240 °C. All analyses have been calculated to 100%. Total iron in the liquids is calculated as Fe^{2+}.

lowest concentration in the C2-1180 °C experiment after an isothermal rest-time of 3h. In addition, Al_2O_3 content exhibits a contrasting behavior since it remains close to the concentration of the starting material in the experiments performed at 1190 °C whereas in the experiments at 1180 °C it reaches a maximum concentration after 3 hours and then it decreases approaching the concentration of the starting material after 15 hours (Figure 7b). The observed trends are coherent with the different mutual abundance and composition of newly crystals, mainly PlgN and Cpx, determined in the respective 1180 °C and 1190 °C charges (ϕPlgN/ϕCpx=0.08 and 0.6 for C2-3h and for C3-

15h runs; ϕPlgN/ϕCpx=1 and 0.85 for C5-3h and for C6-15h runs; f is the area fraction of newly plagioclases and clinopyroxenes determined by image analyses; Table 4).

The glass compositions of the experiments at 1230 and 1240 °C are close to that of the starting material with the exception of the Al_2O_3 concentration, which, considering experiments performed at the same temperature, increases as the dwell time increases up to 10 hours in both the 1230 and 1240 °C isothermal time-series experiments and then its amount remains almost constant (D3-20h and D6-20h runs). Finally, mapping of glass-plagioclase boundary shows no distinct Al-zoning in the crystal or glass (Figure S3 in Supplementary materials).

Plagioclase-melt and clinopyroxene-melt equilibria

Plagioclase-melt equilibria for each experiment has been tested comparing the An content of PlgS/PlgN with the An content of plagioclase predicted to be in equilibrium with the composition of its host experimental glass. The equilibrium plagioclase composition as a function of melt composition has been calculated through the empirical model proposed by Namur et al. (2012), calibrated for anhydrous basalt to rhyolite melts at 1-atm with a reproducibility of ~5%.

Defining the disequilibrium degree as ΔAn ($An_{measured}$ - $An_{calculated}$), equilibrium is at ΔAn = 0. Our calculations show that PlgS slightly diverge from equilibrium conditions as temperature decreases (e.g., for 15h dwell time ΔAn is ~5 at 1200 °C and 12 at 1180 °C; Table S1 in Supplementary materials) while PlgN commonly are close to equilibrium with ΔAn ranging from -4.5 to ~5. An exception is represented by the 1190 °C time-series experiments in which equilibrium PlgN (ΔAn~ -1 in C4 run; ΔAn ~-2 in C5 run and ΔAn~1 in C6 run) coexists with newly plagioclases whose composition slightly deviates from equilibrium with the hosting glass composition (ΔAn~8 in C5 run and ΔAn~11 in C6 run).

Concerning clinopyroxene, the Fe–Mg distribution coefficients between Cpx and melt ($KD(Fe\text{-}Mg)^{Cpx\text{-}liq}$= $Fe_{Cpx}\cdot Mg_{liq}/Mg_{Cpx}\cdot Fe_{liq}$, calculated assuming all Fe as Fe^{2+} in both phases) vary between 0.5 and 0.8, far above the equilibrium range of 0.28±0.08 (Putirka, 2008). This along with the observation that clinopyroxene does not occur in the zero-time experiments at 1190 and 1180 °C (see C1-0h and C4-0h runs) suggests that clinopyroxene formed and rapidly grew at its liquidus temperature in disequilibrium with the melt, and also a rest time under isothermal condition of 15 hours was not sufficient for the crystal-melt equilibrium approaching. On the other hand, the Fe-Mg interdiffusion in clinopyroxene is extremely slow (i.e., 10^{-18}-10^{-22} m^2 s^{-1} along the c-axis depending on temperature and fO_2 conditions, Cherniak and Dimanov, 2010), and even considering a diffusion coefficient of 10^{-18} $m^2\cdot s^{-1}$, at diffusion length scales >1 μm a mineral melt re-equilibrium would require more than a month to be achieved.

DISCUSSION

Experimental results compared with literature phase relations and Rhyolite-MELTS modeling

The sequence of crystallizing phases obtained is oxide ⇒ oxide+plagioclase⇒oxide+plagioclase+clinopyroxene, although experiments on PST9 composition from literature indicate the Plg crystallization subsequent to that of clinopyroxene (Conte et al., 2006; Pichavant et al., 2013; Ni et al., 2014). However, the cited literature experiments were conducted at lower oxygen fugacity conditions than our experiments and a different crystallization sequence could occur.

Results of equilibrium experiments performed on PST9 composition at the same P and fO_2 conditions of our experiments were described by Agostini et al. (2013), which bracket the plagioclase liquidus temperature at ~1190 °C, maybe in coexistence with clinopyroxene although the latter, on the basis of their morphology and zoned composition probably represent restitic crystals (see Figures 3, 5 in Agostini et al., 2013).

From these remarks, the occurrence of plagioclase seed in our charge seems to favor the crystallization of this phase at higher temperature delaying the clinopyroxene appearance. Indeed, the first appearance of the newly plagioclases is at 1220 °C and the first occurrence of Cpx is in the longest experiment at 1200 °C (Table 3). Furthermore, at 1180 °C and run duration of 15 hours in addition to Plg, Cpx and Ox Agostini et al. (2013) observed also the occurrence of olivine in the mineral assemblage, never observed in our experiments.

Finally, we also compared experimental results of the longest experiments, considered those closest to equilibrium conditions, with those obtained by using the software package Rhyolite-MELTS designed for thermodynamic modelling of phase equilibria in magmatic systems (Ghiorso and Sack, 1995; Gualda et al., 2012). The PST9 differentiation modeling were performed constraining the oxygen fugacity to HM+2, a value approaching that of the experimental conditions, and in the temperature range of 1180-1220 °C.

Simulation results (Table S2 in Supplementary materials) show that:

- spinel is the liquidus phase while plagioclase appears after clinopyroxene;
- crystallization temperatures predicted by Rhyolite-MELTS indicate a T of 1210 °C for the onset of clinopyroxene and a T of 1192 °C for plagioclase, shifting them from the experimental ones by 10 °C for clinopyroxene and by 28 °C for plagioclase;

- the predicted plagioclase and clinopyroxene proportions fit quite well the values of the experimental data at the lowest temperature but mismatch with those from run at 1190 °C. Moreover, the code modeling indicates higher amounts of oxides and increase of plagioclase/clinopyroxene ratio with decrease of temperature (Table S3 in Supplementary materials);

- the compositions of experimental oxides deviate from those predicted by Rhyolite-MELTS, while plagioclase and clinopyroxene compositions are relatively better modelled. Linked to the differences on phase proportions and predicted mineral compositions, liquid line evolution resulting by Rhyolite-MELTS mismatches from that of experiments as shown in the Figure S4 (in Supplementary materials) in which the chemical evolution of the residual liquids obtained from the experiments at 3 and 15 hours is compared with those estimated by Rhyolite-MELTS modeling. The following considerations and explanations arise from the comparison: *i*) the less evolved synthetic and model liquids well match with the composition of the natural starting material. *ii*) A different evolutionary trend is identified for the most evolved liquids obtained at 3 and 15 hours, this difference is remarkably evident for Al_2O_3, FeO, MgO and negligible or absent for CaO, Na_2O, K_2O. Such mismatch reflects the significant predominance of clinopyroxene over plagioclase in the 3h-experiment at 1180° C (Table 4), which resulted in the enrichment of Al_2O_3 (incompatible in Cpx), and depletion of FeO and MgO (compatibles in Cpx) in the residual liquid. *iii*) The modeling of the liquid line of descent never matches with those observed in the synthetic glasses, this trend is particularly evident for CaO and FeO. The main remarkable difference between the crystallization observed in the experiments and those estimated by the model is that the amount of oxides is 2-12 times higher in the simulations than in the experiments (Table S3 in Supplementary materials). The higher amounts of oxides in the simulations cause the strong depletion in the FeO contents of the simulated liquids and a consequent early increase of CaO content till the appearance of plagioclase and clinopyroxene.

Effect of pre-existing crystals on nucleation and composition of plagioclase microlites

A first line of evidence of this study is that the occurrences of crystalline seeds in a solidifying K-basalt melt like PST9 *golden* pumice alters the crystallization sequences of phase assemblage forcing the early formation of plagioclase. This could be due to the action of the dissolution process on the plagioclase seeds during the initial annealing step at 1225 °C, which, although not revealed by the chemical map analyses, cannot be ruled out. If the dissolution process has taken place it may have resulted in the formation of a chemical gradient in the melt around the plagioclase seeds, triggering the overgrowth of an only few microns (<<10 μm; Figure S1 in Supplementary materials) plagioclase rim thus causing the metastable extension of plagioclase liquidus (Simakin and Salova, 2004). Beyond that, the irregular shape of the new rims overgrowth on PlgTG observed in the shortest experiments (Larsen, 2005 and references therein), the presence of the early formed oxides as well as the moderate cooling rate applied to the melts (100 °C/h) to reach the experimental temperature, all favored the occurrence of a heterogeneous nucleation process (Fockin et al., 2006; Mollo et al., 2012b; Iezzi et al., 2014). In addition, since *i*) the formation of metastable phases requires a lower activation energy than that required for the formation of thermodynamically stable phases (Kirkpatrick, 1983; Lasanga, 1997; Zang, 2008; Iezzi et al., 2011, 2014 and references therein) and, *ii*) under dynamic conditions of crystallization, Al-rich minerals are more favored to nucleate (Kirkpatrick, 1983; Hammer, 2008; Iezzi et al., 2008; Del Gaudio et al., 2010; Mollo et al., 2011; Iezzi et al., 2011, 2014), this may also account for the observed formation of the plagioclase earlier than that of the clinopyroxene.

As regards the nucleation rate of newly plagioclases (J_{PlgN}; Table 4), the obtained range of variability (10^2-10^5 $cm^{-3}\cdot s^{-1}$) fully matches the range estimated by Arzilli et al. (2015) for plagioclases crystallized from the isothermal single-step decompression experiments performed by Agostini et al. (2013) on PST9 composition. In agreement with the findings of Arzilli et al. (2015), who observed a general decrease of the minimum nucleation rate with increasing undercooling and experimental dwell time, in our experiments we noted an exponentially decrease of J_{PlgN} with increasing experimental time (Figure 8). This exponential decay is more enhanced for the experiments conducted at the high temperatures, i.e. 1190 and 1200 °C, compared to those performed at the lowest temperature (1180 °C). Moreover, the gap in the nucleation rate between the high and low temperature experiments is maximum, i.e. more than two orders of magnitude, at the experimental times of 0 hours, tends to be reduced to one order of magnitude after 3 hours and is on the same order of magnitude after 15 hours. These observations imply that the runs performed at 1190 and 1200 °C are the most favorable for the nucleation of new plagioclase crystals at the beginning of the experiments. However, most of these nuclei are thermodynamically unstable and they tend to be reabsorbed in the evolving residual liquid as testified by the lowering of the nucleation rate after 3 hours. Moreover, the longest runs are characterized by the lowest nucleation rates as well as minimal gaps between the experiments performed at the different temperatures

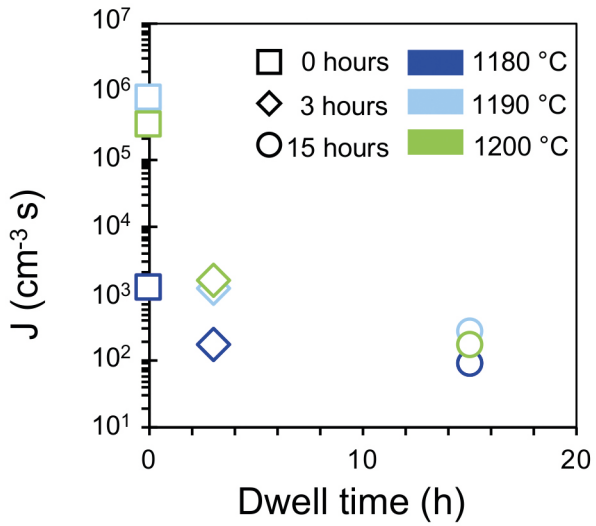

Figure 8. Nucleation rate (*J*) plotted against the isothermal dwell time of experiments.

suggesting that all the unstable nuclei have been resorbed and that since now the growth of the residual nuclei is more favored than the nucleation of new crystals (Table S4 in Supplementary materials).

Lastly, a higher nucleation rate of plagioclase nucleation from PST9 melt obtained at ΔT<45 °C was also observed by Arzilli et al. (2015) and, as emphasized by these authors, this behavior is in contrast to what observed in many other studies, according to which the nucleation process is favored by high ΔT (e.g., Couch et al. 2003; Hammer and Rutherford, 2002; Mollard et al., 2012; Shea and Hammer, 2013). Our results support one of the possible explanations proposed by Arzilli et al. (2015) for the observed discrepancy on plagioclase nucleation behavior, concerned the presence of pre-existing minerals that promoted the heterogeneous nucleation regime imposing a metastable condition at the system (change of sequence of crystallization) for ΔT<45 °C.

A notable outcome from our experiments concerns the composition of the newly plagioclases that in the long experiments, i.e. 3 and 15 hours, performed at 1190 °C are characterized by the presence of two compositional populations. One in equilibrium with the residual melt having composition respectively $Ab_{28}An_{68}Or_4$ in the run at 3 hours and $Ab_{29}An_{68}Or_3$ in the run at 15 hours and the second more calcic ($Ab_{20}An_{78}Or_2$ in both runs) in disequilibrium with the coexisting liquid. Moreover, the plagioclase crystals in equilibrium are richer in SiO_2, TiO_2, and poorer in Al_2O_3, FeO, MgO than those in disequilibrium. The plagioclase in disequilibrium are particularly enriched in FeO with an iron content that is more than the double of those of the plagioclase in equilibrium (2.4 wt% vs ~1 wt%). It should also be noted that the composition of plagioclases in disequilibrium closely mirrors that of the overgrown rims (Table S1 in Supplementary materials). The shortest run is characterized only by a single population of plagioclase crystals in equilibrium with the residual melt. Interestingly, these crystals have a composition that is intermediate ($Ab_{25}An_{72}Or_3$, FeO=1.8 wt%) between those of plagioclase in equilibrium and disequilibrium found in the longest runs. These crystals are also slightly enriched in MgO than those in the longest runs. We suggest that the presence of a single or double population of plagioclase crystals is strictly related to the onset of clinopyroxene crystallization. The shortest run does not crystallize clinopyroxene and it is characterized by only a single population of plagioclase in equilibrium with the residual melt. The longest runs crystallize clinopyroxene and they are characterized by two plagioclase populations. Obviously, plagioclase is the first phase to appear and after 3 hours it is joined by the appearance of clinopyroxene. We suggest that the most calcic and Fe-rich plagioclase, i.e. those in disequilibrium, represent the crystallization of plagioclase before the appearance of clinopyroxene whereas those in equilibrium co-crystallize together with clinopyroxene. To support this idea we note *i*) that elements incompatible in both mineral phases (Si and e.g., K) tend to increase their concentration in the plagioclase in equilibrium, i.e. those that co-crystallize with clinopyroxene; *ii*) Al that is compatible in plagioclase but incompatible in clinopyroxene tends to decrease its concentration in the co-crystallizing plagioclase according to the fact that it is already depleted in the residual melt given the crystallization of plagioclase in disequilibrium; *iii*) elements that are compatible in clinopyroxene (Fe, Mg) but incompatible in plagioclase tend to decrease their concentration in the co-crystallizing plagioclase; *iv*) Ca that is compatible in both phases tends to decrease its concentration in the co-crystallizing plagioclase; *v*) Na that is incompatible in clinopyroxene changes its behavior from incompatible in the most calcic non in equilibrium plagioclase to compatible in the co-crystallizing in equilibrium plagioclase.

In the experiments at 1180 °C, instead, a single compositional population approaching to crystal-melt equilibrium of PlgN was found, even in the long experiments (ΔAn~6 in 3h-long run, C2, and ΔAn~3.5 in 15h long run, C3) while the An-Fe rich plagioclase type appears to develop only as overgrown rim of seed. This suggests that the runs at 1180 °C are probably closer to an equilibrium condition whereby, once the resting temperature of 1180 °C is reached, clinopyroxene+plagioclase cotectic crystallization begins, as indicated by equilibrium experiments and thermodynamic modeling.

Influence of pre-existing minerals on crystals growth rate

Plagioclase

Plagioclase growth rates calculated measuring overgrown rims closely approximate those calculated measuring microlite sizes although the values of the latter are slightly higher (Figure S5a in Supplementary materials) decreasing both up to two orders of magnitude increasing the experimental dwell time (Table 4). Furthermore, the effect of the occurrence of pre-existing crystals in a melt on plagioclase growth rates is visible from the experiments quenched upon reaching the target temperature, in which ΔT shows a linear correlation with G_{PlgN} but not with G_{PlgS} (Figure S5b in Supplementary materials).

Calculated PlgN growth rates fit the range obtained in previous experimental studies on PST9 rock (G= 10^{-6}-10^{-8} cm·s^{-1}; Conte et al., 2006; Agostini et al., 2013; Arzilli et al., 2015). In particular, with respect these studies that obtained the highest G values of ~10^{-6} cm·s^{-1} from the high undercooling (ΔT≥80 °C) - fast cooled experiments, we estimated the same order of magnitude for G from experiments at ΔT≤45 °C and dwell time of 0h. G_{PlgN} determined for long lasting experiments (3h and 15 h) match well those estimated by Agostini et al. (2013), 10^{-7}-10^{-8} cm·s^{-1}, for the same ΔT range (ΔT≤46 °C) while, they are approximately one order of magnitude higher compared to the G data determined for plagioclases crystallized from an anhydrous potassic trachybasalt from Mt. Etna, in experiments similar to ours both for design and ΔT-P-fO_2 conditions (Orlando et al., 2008). In particular, these authors provide growth rates, calculated measuring both the size of newly plagioclase microlites and the wideness of rim overgrown on the plagioclase seeds, that are in the order of 10^{-8} cm·sec^{-1} for experiments at ΔT≤20 °C and values of 10^{-9} cm·s^{-1} in experiments at higher undercooling. It should be noted that the slowest growth rates (<10^{-8} cm·s^{-1}) are linked to long experimental duration (≥15 h) and then the calculated G could be apparent which means that the system is approaching conditions near to the textural equilibrium (e.g., Couch, 2003; Arzilli et al., 2015; Bonechi et al., 2020).

Clinopyroxene

By focusing on clinopyroxenes nucleated and grown from melts of similar alkaline composition (Figure 9), the growth rates resulting from our experiments (8.4·10^{-8}-2.0·10^{-7} cm·s^{-1}) are higher than those estimated for Mt. Etna trachybasalt (1.8·10^{-9}-4.6·10^{-8} cm·s^{-1}; Orlando et al., 2008), and, for comparable experimental dwell time, higher than those determined by Bonechi et al. (2020) for subhedral to euhedral clinopyroxenes crystallized from an anhydrous/hydrous K-basaltic rock from Campi Flegrei Volcanic District (~1·10^{-8}-~5·10^{-8} cm·s^{-1}; Figure 9). Our data instead, are in the trend of Gs that Pontesilli et al. (2019) determined through 2-24 hours, isothermal time-series experiments on a starting material composition reproducing trachybasalt products of Mt. Etna (5·10^{-8}-4.7·10^{-7} cm·s^{-1}). The mismatch of G data between the two studies using Mt. Etna as starting composition has been attributed by Bonechi et al. (2020) to the difference in the respective experimental setup that influenced the mechanism of a silicate melt crystallization i.e., how the melt is forced into disequilibrium conditions (supersaturation in a mineral phase) and the rate at which it can return to equilibrium through nucleation and growth of crystals (e.g. Kirkpatrick, 1981; Ni et al., 2014; Befus and Andrews, 2018; Pontesilli et al., 2019 and references herein): static, low undercooling (ΔT=10-30 °C) experiments of Orlando et al. (2008) versus dynamic experiments of Pontesilli et al. (2019) at high cooling rate (80 °C/min) and high undercooling conditions (ΔT=80-120 °C). Moreover, the comparison between our and Orlando et al. (2008) G data demonstrates how the mechanism of melt crystallization can be further complicated by the presence and type of antecrysts in the system, as they can reduce or inhibit the initial supersaturation of a specific mineral phase. Figure 9 shows that the variation of G_{Cpx} as function of dwell time calculated in this study is upwards shifted respect to the trend defined by G data from Orlando et al. (2008), despite the similar conditions of moderate cooling rate and low undercooling. The mismatch between the two studies can be explained by the fact that in Orlando et al. (2008) G_{Cpx} were evaluated only on Cpx seeded experiments, whereas in our experiments the added plagioclases seeds induced a metastable condition leading a delay in the crystallization of clinopyroxene. The kinetic effects of such disequilibrium condition are clearly evident in the experiments at 1180 °C and in particular in the high amount of clinopyroxene (ϕ_{Cpx}=21%; Table 4) present in the charge maintained isothermally for 3h (Figure 5b). The low degree of undercooling (ΔT=45 °C) probably allowed the maintenance of an interface-limited crystal growth regime, preventing the formation of dendritic clinopyroxenes (Pontesilli et al., 2019 and references therein). In the experiment at the resting time of 15h the size of clinopyroxene increases significantly developing even epitaxial growth (Figure 5c).

In the longest experiments the observed coarsening and grow of clinopyroxene appears to be related to the achievement of near textural equilibrium conditions in agreement with what has been documented by several authors, namely that the textural maturation of clinopyroxene is rapid (i.e., 20-24h; Burkhard, 2005; Mollo et al., 2011; Mollo et al., 2013; Pontesilli et al.,

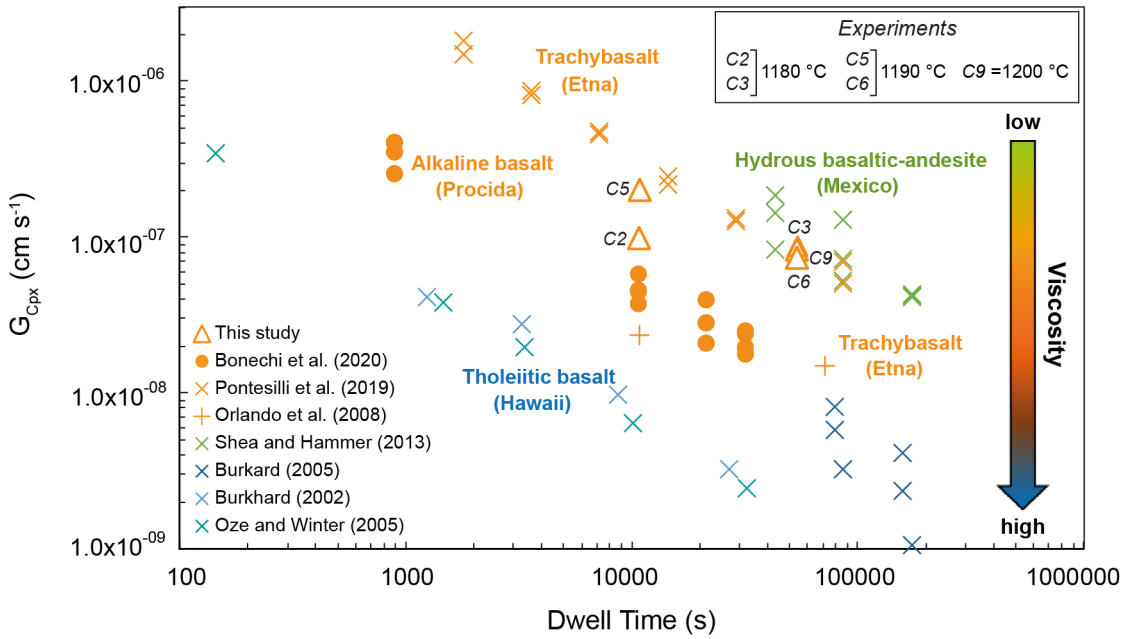

Figure 9. Diagram showing the experimental duration (s) versus the crystal growth rate (G) for this and previous studies on clinopyroxene, modified after Bonechi et al. (2020). The symbol colors of the data plotted in the graph are consistent with the degree of viscosity of the starting materials, calculated as crystal-free melts (see the color scale of the arrow on the right), used in the respective experimental studies. Viscosity calculations were made according to Vona et al. (2011). For comparable experimental dwell times note the higher G_{Cpx} values calculated for the current and Pontesilli et al. (2019) studies than those evaluated from the studies of Orlando et al. (2008) and Bonechi et al. (2020). Despite the compositional similarity of the starting materials used in these works, these apparent discrepancies are due to the different undercooling and cooling rate of the investigated systems (static vs dynamic experiment) as well as to the presence/absence of added mineral seeds.

2019). Therefore, the growth rate calculated from these runs (G_{Cpx}=7.4-8.8·10^{-8} cm·s^{-1}) could be apparent although, experiments longer than 15h would be needed to verify this.

Plagioclase seed dissolution and formation of hybrid melts

BSE photomicrographs show that at T>1225 °C plagioclase seed was affected by dissolution but an estimation of the dissolution rates is valuable only for the experiments which the isothermal step is longer than 3h. Calculations indicate that the dissolution rate in the same order of magnitude for both 1230 and 1240 °C temperatures (10^{-9} cm·s^{-1}). D-values can be directly compared with those estimated in dissolution experiments similar to ours for set up and T-P-fO_2 conditions by Agostini et al. (2013). The D estimated by these authors turn out to be two orders of magnitude higher (D~10^{-7} cm·s^{-1}) for experiments of similar isothermal resting times as ours (≥10 h). The more sodic labradoritic (An_{64-67}) zoned plagioclase seeds used in the study of Agostini et al. (2013) with respect to the homogeneous bytownitic crystals (An_{76-78}) chosen for our experiments likely account for the significant difference in D estimations between the two studies considering that for a same melt composition, the dissolution rate of plagioclase increases as An content in plagioclase decreases (Tsuchiyama, 1985).

Finally, the enrichment in plagioclase components (e.g., Al_2O_3; Figure 7) already observable in the glass produced by the shortest dissolution runs suggests that in the investigated system, the processes of dissolution and melting appear favored and even modest degrees of superheat can result in a relatively rapid contamination of the melt.

Plagioclase cannibalization in the Stromboli magmatic system

The textural and compositional complexity of the minerals cargo of crystal-rich magma erupted from Stromboli allowed many authors to reconstruct the processes occurring within the plumbing system of the volcano (e.g. see Landi et al., 2022 and references therein).

Plagioclase compositions crystallized from the experiments of Agostini et al. (2013) indicate that the

natural crystal-rich PST9-like magma is in equilibrium with labradoritic plagioclases (An_{60-70}), and that they should form at a pressure below the 25 MPa i.e., in the shallow part of Stromboli's magmatic system. The natural plagioclase phenocrysts exhibit concentric zoning made up of alternating bytownitic and labradoritic layers which the outermost zone (up to 150 μm thick) is labradoritic (An_{62-70}), interpreted as the record of multiple crystallization and dissolution events (Landi et al., 2022 and references therein). Microphenocrystals of 100-200 μm in size, on the other hand, do not show features attributable to a dissolution process and sometimes they show an abrupt compositional change from a bytownite core to a labradorite rim (Armienti et al., 2007). A similar net change in plagioclase composition is observed in the PlgN crystallized in our time-series experiments at 1180-1190 °C. Highlighting how the "cannibalization" of plagioclase crystals from a resident crystal mush by an ascending PST9-like magma, may induce a delay in the clinopyroxene crystallization in favor of bytownitic plagioclases until the metastable conditions are no longer sustainable by the system and clinopyroxene co-crystallizes along with labradoritic plagioclase. The sudden crystallization of clinopyroxene is clearly evident at 1180 °C where the high amount of clinopyroxene (ϕ_{Cpx}=21%; Table 4) can induce a drastic increase of magma's viscosity (~ two order of magnitude calculated according to Vona et al., 2011). This could affect the mobility of gas flow at very shallow levels, contributing to create in a very short time, transient conditions of conduit pressurization, which can trigger more energetic events than the normal volcanic activity (Viccaro et al., 2021; Landi et al., 2022).

CONCLUSIONS

Our experimental results document the influence induced by the presence of pre-existing minerals different from the liquidus one, on the crystallization kinetics of a magmatic system even at low degree of undercooling (5≤ ΔT≤45 °C). The main results of this study indicate that for a moderate cooling rate, the presence of antecrysts/xenocrysts of plagioclase in the PST9 potassic basalt:

i) facilitates the heterogeneous nucleation of new plagioclases by delaying the appearance of the clinopyroxene, the liquidus phase under equilibrium and dynamic crystallization conditions. However, the decrease in nucleation lag of clinopyroxene by increasing the DT and the significant decrease in the plagioclase nucleation rate estimated for 0-hours experiment at 1180 °C suggests that the metastable extension of plagioclase liquidus is less efficient for undercooling ≥35 °C;

ii) produces a greater effect on the growth rate of clinopyroxene than on that of plagioclase due to disequilibrium induced by the early crystallization of newly plagioclases, which in turn caused an oversaturation in clinopyroxene in the system;

iii) affects composition of the newly plagioclases that show a marked change from bytownite to labradorite as clinopyroxene crystallizes;

iv) induces the main deviation from the equilibrium liquid line of descent for ΔT>35 °C;

v) if the composition of plagioclase antecrysts/xenocrysts is close to that of plagioclase in equilibrium with the surrounding melt, the dissolution and melting of the crystals may be triggered even for low overheating contaminating quickly the melt.

ACKNOWLEDGEMENTS

Authors wish to thank an anonymous reviewer for his constructive comments on the earlier version of the manuscript. The authors would also like to thank M. Albano and M. Paciucci (CNR-IGAG) for help in electronic backscattered images and EDS multi-element chemical maps. M. Serracino (CNR-IGAG) is warmly thanked for his help in EMP analyses. This research was supported by the Grant Agency of Czech Republic (GAČR, grant number 23-04734S to AF).

REFERENCES

Agostini C., Fortunati, A., Arzilli, F., Landi, P., Carroll, M.R., 2013. Kinetics of crystal evolution as a probe to magmatism at Stromboli (Aeolian Archipelago, Italy). Geochimica et Cosmochimica Acta 110, 135-151.

Arzilli F., Agostini C., Landi P., Fortunati A., Mancini L., 2015. Plagioclase nucleation and growth kinetics in a hydrous basaltic melt by decompression experiments. Contribution to Mineralogy and Petrology 170 (5-6), 55.

Arzilli F., Polacci M., La Spina G., Le Gall N., Llewellin E.W., Brooker R.A., Torres-Orozco R., Di Genova D., Neave D.A., Hartley M.E., Mader H.M., Giordano D., Atwood R.C., Lee P.D., Burton M.R., 2022. Dendritic crystallization in hydrous basaltic magmas controls magma mobility within the Earth's crust. Nature Communication 13, 3354. https://doi.org/10.1038/s41467-022-30890-8.

Befus K.S. and Andrews B.J., 2020. Crystal nucleation and growth produced by continuous decompression of Pinatubo magma. Contribution to Mineralogy and Petrology 173, 92 https://doi.org/10.1007/s00410-018-1519-5.

Bergantz G. W., Schleicher J.M., Burgisser A., 2015. Open-system dynamics and mixing in magma mushes. Nature Geoscience 8, 793-796.

Bonechi B., 2020. Influence of pre-existing nuclei on the crystallization kinetics of primitive alkaline magmas: insights on the deep feeding system of the Campi Flegrei Volcanic District. Minerals, 10, 234.

Bonechi B., Perinelli C., Gaeta M., 2020a. Clinopyroxene growth rates: high-pressure investigation on a primitive

alkaline basalt from the Campi Flegrei Volcanic District (south Italy). Bulletin of Volcanology 82, 5.

Bonechi B., Perinelli C., Gaeta M., Tecchiato V., Fabbrizio A., 2020b. Amphibole growth from a primitive alkaline basalt at 0.8 GPa: time-dependent compositional evolution, growth rate and competition with clinopyroxene. Lithos 354-355, 105272.

Bonechi B., Perinelli C., Gaeta M., Fabbrizio A., Petrelli M., Strand L., 2021a. High pressure trace element partitioning between clinopyroxene and alkali basaltic melts. Geochemica et Cosmochimica Acta 305, 282-305.

Bonechi B., Perinelli C., Gaeta M., Stagno V., Fabbrizio A., Mollo S., Hrubiak R., 2021b. High pressure experimental investigation of clinopyroxene dissolution in a K-basaltic melt. Chemical Geology 584, 120533.

Brearley M. and Scarfe C.M., 1986. Dissolution rates of upper mantle minerals in an alkali basalt melt at high pressure: an experimental study and implications for ultramafic xenolith survival. Journal of Petrology 27, 1157-1182. https://doi.org/10.1093/petrology/27.5.1157.

Burkhard D.J.M., 2005. Nucleation and growth rates of pyroxene, plagioclase, and Fe-Ti oxides in basalt under atmospheric conditions. European Journal of Mineralogy 17, 675-685.

Cashman K.V., 1990. Textural constraints on the kinetics of crystallization of igneous rocks. Reviews in Mineralogy 24, 259-314.

Cashman K.V., Sparks R.S.J., Blundy J.D., 2017. Vertically extensive and unstable magmatic systems: a unified view of igneous processes. Science 355, eaag3055. doi:10.1126/science. aag3055.

Chen Y. and Zhang Y., 2008. Olivine dissolution in basaltic melt. Geochimica et Cosmochimica Acta 72, 4756-4777. https://doi.org/10.1016/j.gca.2008.07.014.

Chen Y. and Zhang Y., 2009. Clinopyroxene dissolution in basaltic melt. Geochimica et Cosmochimica Acta 73, 5730-5747. https://doi.org/10.1016/j.gca.2009.06.016.

Cherniak D. J. and Dimanov A., 2010. Diffusion in pyroxene, mica and amphibole. Reviews in Mineralogy and Geochemistry 72, 641-690.

Conte A.M., Perinelli C., Trigila R., 2006. Cooling kinetics experiments on different Stromboli lavas: Effects on crystal morphologies and phases composition. Journal of Volcanology and Geothermal Research 155, 179-200.

Couch S., 2003. Experimental investigation of crystallization kinetics in a haplogranite system. American Mineralogist 88, 1471-1485.

Couch S., Sparks R.S.J., Carroll M.R., 2003. The kinetics of degassing induced crystallisation at Soufriere Hills volcano, Montserrat. Journal of Petrology 44, 1477-1502.

Del Gaudio P., Mollo S., Ventura G., Iezzi G., Taddeucci J., Cavallo A., 2010. Cooling rate induced differentiation in anhydrous and hydrous basalts at 500 MPa: implications for the storage and transport of magmas in dikes. Chemical Geology 270, 164-178.

Di Fiore F., Mollo S., Vona A., MacDonald A., Ubide T., Nazzari M., Romano C., Scarlato P., 2021. Kinetic partitioning of major and trace cations between clinopyroxene and phonotephritic melt under convective stirring conditions: New insights into clinopyroxene sector zoning and concentric zoning. Chemical Geology 584, 120531. https://doi.org/10.1016/j.chemgeo.2021.120531.

Donaldson C.H., 1976. An experimental investigation of olivine morphology. Contribution to Mineralogy and Petrology 57, 187-213.

Donaldson C.H., 1985. The rates of dissolution of Olivine, Plagioclase, and Quartz in a Basalt Melt. Mineralogical Magazine 49, 683-693. https://doi.org/10.1180/minmag.1985.049.354.07.

Dunbar N.W., Jacobs G.K., Naney M.T., 1995. Crystallization processes in an artificial magma: variations in crystal shape, growth rate and composition with melt cooling history. Contribution to Mineralogy and Petrology 120, 412-425.

Fokin V.M., Zanotto E.D., Yuritsyn N.S., Schmelzer, J.W.P., 2006. Homogeneous crystal nucleation in silicate glasses: a 40 years perspective. Journal of Non-Crystalline Solids 352, 2681-2714.

Ganovex Team, 1987. Geological map of North Victoria land, Antarctica, 1:500 000 - Explanatory Notes - Geologisches Jahrbuch B66, 7-79.

Giuliani L., Iezzi G., Vetere F., Behrens H., Mollo S., Cauti F., Ventura G., Scarlato P., 2020. Evolution of textures, crystal size distributions and growth rates of plagioclase, clinopyroxene and spinel crystallized at variable cooling rates from a mid-ocean ridge basaltic melt. Earth-Science Reviews. https://doi.org/10.1016/j.earscirev.2020.103165.

Gualda G.A.R., Ghiorso M.S., Lemons R.V., Carley T.L., 2012. Rhyolite-MELTS: a modified calibration of MELTS optimized for silica-rich, fluid-bearing magmatic systems. Journal of Petrology 53, 875-890. https://doi.org/10.1093/petrology/egr080.

Hammer J.E. and Rutherford M.J., 2002. An experimental study of the kinetics of decompression-induced crystallization in silicic melt. Journal of Geophysical Research Solid Earth 107 (B1) (ECV-8).

Hammer J.E., 2008. Experimental studies of the kinetics and energetics of magma crystallization. Reviews in Mineralogy and Geochemistry 69, 9-59. https://doi.org/10.2138/rmg.2008.69.2.

Hersum T.G. and Marsh B.D., 2006. Igneous microstructures from kinetic models of crystallization. Journal of Volcanology and Geothermal Research 154, 34-47.

Higgins M.D., 1998. Origin of anorthosite by textural coarsening: quantitative measurements of a natural sequence of textural development. Journal of Petrology 39, 1307-1323.

Higgins M.D., 2006. Quantitative textural measurements in

igneous and metamorphic petrology. Cambridge University Press, Cambridge.

Huber C., Bachmann O., Dufek J., 2012. Crystal-poor versus crystal-rich ignimbrites: A competition between stirring and reactivation. Geology 40 (2), 115-118. https://doi.org/10.1130/G32425.1.

Johannes W., Koepke J., Behrens H., 1994. Partial melting reactions of plagioclase and plagioclase bearing systems. In: Feldspar and Their Reactions. (Ed.): I. Parson, Kluwer Dordrecht, 161-194.

Iezzi G., Mollo S., Torresi G., et al., 2011. Experimental solidification of an andesitic melt by cooling. Chemical Geology 283, 261-273. https://doi.org/10.1016/j.chemgeo.2011.01.024.

Iezzi G., Mollo S., Shaini E., Cavallo A., Scarlato P., 2014. The cooling kinetics of plagioclase revealed by electron microprobe mapping. American Mineralogist. https://doi.org/10.2138/am.2014.4626.

Kahl M., Chakraborty S., Costa F., Pompilio M., 2011. Dynamic plumbing system beneath volcanoes revealed by kinetic modeling, and the connection to monitoring data: An example from Mt. Etna. Earth and Planetary Science Letters 308, 11-22.

Kerr R.C., 1995. Convective crystal dissolution. Contribution to Mineralogy and Petrology 121, 237-246. https://doi.org/10.1007/BF02688239.

Kirkpatrick R.J., 1981. Kinetics of crystallization of igneous rocks. In: (Eds.), A.C. Lasaga, R.J. Kirkpatrick, Reviews in Mineralogy 8, 321-395.

Kuo L.C. and Kirkpatrick R.J., 1985a. Dissolution of mafic minerals and its implications for the ascent velocities of peridotite-bearing basaltic magmas. Journal of Geology 93, 691-700. https://doi.org/10.1086/628996.

Kuo L.C. and Kirkpatrick R.J., 1985b. Kinetics of crystal dissolution in the system: diopside- forsterite-silica. American Journal of Science 285, 51-90. https://doi.org/10.2475/ajs.285.1.51.

Landi P., D'Oriano C., Petrelli M., Nazzari M., Andronico D., 2022. Inferences on the magmatic plumbing system at Stromboli volcano (Italy) from trace element geochemistry of matrix glasses and minerals in different types of explosive eruptions. Contribution to Mineralogy and Petrology 177, 96. https://doi.org/10.1007/s00410-022-01962-1.

Larsen J.F., 2005. Experimental study of plagioclase rim growth around anorthite seed crystals in rhyodacitic melt. American Mineralogist 90, 417-427.

Lasanga A.C., 1997. Kinetic Theory in the Earth Sciences. Princeton University Press, Princeton, New Jersey, p. 811

Laumonier M., Laporte D., Faure F., Provost A., Schiano P., Ito K., 2019. An experimental study of dissolution and precipitation of forsterite in a thermal gradient: implications for cellular growth of olivine phenocrysts in basalt and melt inclusion formation. Contributions to Mineralogy and Petrology 174, 94.

Le Maitre R.L., Streckeisen A., Zanettin B., 2002. Igneous rocks. A classification and glossary of terms. Recommendations of the IUGS Subcomission on the Systematics of Igneous Rocks.

Liang, Y., 2000. Dissolution in molten silicates: effects of solid solution. Geochimica et Cosmochimica Acta 64, 1617-1627. https://doi.org/10.1016/S0016-7037(00)00331-8.

Liang Y., 2003. Kinetics of crystal-melt reaction in partially molten silicates: 1. Grain scale processes. Geochemistry, Geophysics, Geosystems 4, 1045. https://doi.org/10.1029/2002GC000375.

Lofgren G.E., 1974. An experimental study of plagioclase morphology: isothermal crystallization. American Journal of Science 264, 243-273.

Lofgren G.E., 1980. Experimental studies on the dynamic crystallization of silicate melts, Chapter 11. In: Physics of Magmatic Processes. (Ed.): R.B. Hargraves. Princeton University Press, Princeton, New Jersey.

Lofgren G.E., 1983. Effect of heterogeneous nucleation on basaltic textures: a dynamic crystallization study. Journal of Petrology 24, 229-255. https://doi.org/10.1093/petrology/24.3.229.

Lundgard K.L. and Tegner C., 2004. Partitioning of ferric and ferrous iron between plagioclase and silicate melt. Contribution to Mineralogy and Petrology 147, 470-483.

Maclennan J., 2019. Mafic tiers and transient mushes: evidence from Iceland. Philosophical Transactions of the Royal Society A 377, 20180021. http://dx.doi.org/10.1098/rsta.2018.0021.

Masotta M., Pontesilli A., Mollo S., Armienti P., Ubide T., Nazzari M., Scarlato P., 2020. The role of undercooling during clinopyroxene growth in trachybasaltic magmas: Insights on magma decompression and cooling at Mt. Etna volcano. Geochemica et Cosmochimica Acta 268, 258-276. https://doi.org/10.1016/j.gca.2019.10.009.

Mollo S., Putirka K., Iezzi G., Del Gaudio P., Scarlato P., 2011. Plagioclase-melt (dis)equilibrium due to cooling dynamics: implications for thermometry, barometry and hygrometry. Lithos 125, 221-235.

Mollo S., Misiti V., Scarlato P., Soligo M., 2012a. The role of cooling rate in the origin of high temperature phases at the chilled margin of magmatic intrusions. Chemical Geology 322-323, 28-46.

Mollo S., Iezzi G., Ventura G., Cavallo A., Scarlato P., 2012b. Heterogeneous nucleation mechanisms and formation of metastable phase assemblages induced by different crystalline seeds in a rapidly cooled andesitic melt. Journal of Non-Crystalline Solids 358, 1624-1628.

Mollo S., Putirka K., Misiti V., Soligo M., Scarlato P., 2013. A new test for equilibrium based on clinopyroxene-melt pairs: Clues on the solidification temperatures of Etnean alkaline melts at post-eruptive conditions. Chemical Geology 352, 92-100.

Mollo S., Blundy J., Scarlato P., Iezzi G., Langone A., 2013a. The partitioning of trace elements between clinopyroxene and

trachybasaltic melt during rapid cooling and crystal growth. Contribution to Mineralogy and Petrology 166, 1633-1654. https://doi.org/10.1007/s00410-013-0946-6.

Mollo S. and Hammer J.E., 2017. Dynamic crystallization in magmas. In: EMU Notes in Mineralogy 16, 373-418.

Moore A., Coogan L.A., Costa F., Perfit M.R., 2014. Primitive melt replenishment and crystal-mush disaggregation in the weeks preceding the 2005-2006 eruption, 9°50'N, EPR. Earth and Planetary Science Letters 403, 15-26.

Morgan Z. and Liang Y., 2003. An experimental and numerical study of the kinetics of harzburgite reactive dissolution with applications to dunite dike formation. Earth and Planetary Science Letters, 59-74. https://doi.org/10.1016/S0012-821X(03)00375-3.

Namur O., Charlier B., Toplis M.J., Vander Auwera J., 2011. Prediction of plagioclase-melt equilibria in anhydrous silicate melts at 1-atm. Contribution to Mineralogy and Petrology 163, 133e150. https://doi.org/10.1007/s00410-011-0662-z.

Neave D.A., Passmore E., Maclennan J., Fitton G., Thordarson T., 2013. Crystal-melt relationships and the record of deep mixing and crystallization in the AD 1783 Laki eruption, Iceland. Journal of Petrology 54, 1661-1690. https://doi.org/10.1093/ petrology/egt027.

Nelson S.T. and Montana A., 1992. Sieve textured plagioclases in volcanic rocks produced by rapid decompression. American Mineralogist 77, 1242-1249.

Ni H., Keppler H., Walte N., Schiavi F., Chen Y., Masotta M., Li Z., 2014. In situ observation of crystal growth in a basalt melt and the development of crystal size distribution in igneous rocks.

Orlando A., D'Orazio M., Armienti P., Borrini D., 2008. Experimental determination of plagioclase and clinopyroxene crystal growth rates in an anhydrous trachybasalt from Mt Etna (Italy). European Journal of Mineralogy 20, 653-664.

Passmore E., Maclennan J., Fitton G., Thordarson T., 2012. Mush disaggregation in basaltic magma chambers: evidence from the AD 1783 Laki eruption. Journal of Petrology 53, 2593-2623. https://doi.org/10.1093/petrology/egs061.

Pichavant M., Pompilio M., D'Oriano C., Di Carlo I., 2011. Petrography, mineralogy and geochemistry of a primitive pumice from Stromboli: implications for the deep feeding system. European Journal of Mineralogy 23, 499-517.

Pontesilli A., Masotta M., Nazzari M., Mollo S., Armienti P., Scarlato P., Brenna M., 2019. Crystallization kinetics of clinopyroxene and titanomagnetite growing from a trachybasaltic melt: new insights from isothermal time-series experiments. Chemical Geololy 510, 113-129. https://doi.org/10.1016/j.chemgeo.2019.02.015.

Pupier E., Duchene S., Toplis M.J., 2008. Experimental quantification of plagioclase crystal size distribution during cooling of basaltic liquid. Contribution to Mineralogy and Petrology 155, 555-570.

Putirka K.D., 2008. Thermometers and Barometers for Volcanic Systems. Reviews in Mineralogy and Geochemistry 69, 61-120.

Scarfe C.M., Takahashi E., Yoder Jr.H.S., 1980. Rates of dissolution of upper mantle minerals in an alkali-olivine basalt melt at high pressure. In: Carnegie Inst. Washington Yearbook, 290-296.

Shea T. and Hammer J.E., 2013. Kinetics of cooling- and decompression-induced crystallization in hydrous mafic-intermediate magmas. Journal of Volcanology and Geothermal Research 260, 127-145.

Simakin A.G. and Salova T.P., 2004. Plagioclase Crystallization from a Hawaiitic Melt in Experiments and in a Volcanic Conduit. Petrology 12, 82-92.

Simakin A.G. and Bindeman I.N., 2008. Evolution of crystal sizes in the series of dissolution and precipitation events in open magma systems. Journal of Volcanology and Geothermal Research 177, 997-1010. https://doi.org/10.1016/j.jvolgeores.2008.07.012.

Streck M.J., 2008. Mineral textures and zoning as evidence for open system processes. In: Minerals, Inclusions and Volcanic Processes. (Eds.): K.D. Putirka, F.J.III. Tepley. Mineralogical Society of America and Geochemical Society, Reviews in Mineralogy and Geochemistry 69, 595-622.

Thomson A.R. and Maclennan J., 2013. The distribution of olivine compositions in Icelandic basalts and picrites. Journal of Petrology 54, 745-768. doi:10.1093/petrology/egs083.

Tsuchiyama A., 1985. Dissolution kinetics of plagioclase in the melt of the system diopside-albite-anorthite, and origin of dusty plagioclase in andesites. Contribution to Mineralogy and Petrology 89, 1-16.

Tsuchiyama A., 1986. Melting and dissolution kinetics: application to partial melting and dissolution of xenoliths. Journal of Geophysical Research 91, 9395-9406. https://doi.org/10.1029/JB091iB09p09395.

Tsuchiyama A. and Takahashi E., 1983. Melting kinetics of a plagioclase feldspar. Contribution to Mineralogy and Petrology 84, 345-354.

Tursack E. and Liang Y., 2012. A comparative study of melt-rock reactions in the mantle: laboratory dissolution experiments and geological field observations. Contribution to Mineralogy and Petrology 163, 861-876. https://doi.org/10.1007/s00410-011-0703-7.

Van Orman J.A. and Grove T.L., 2000. Origin of lunar high-titanium ultramafic glasses: constraints from phase relations and dissolution kinetics of clinopyroxene-ilmenite cumulates. Meteoritics & Planetary Science 35, 783-794. https://doi.org/10.1111/j.1945-5100.2000.tb01462.x.

Viccaro M., Giacomoni P.P., Ferlito C., Cristofolini R., 2010. Dynamics of magma supply at Mt. Etna volcano (Southern Italy) as revealed by textural and compositional features of plagioclase phenocrysts. Lithos 116, 77-91.

Viccaro, M., Cannata, A., Cannavò, F., De Rosa R., Giuffrida M., Nicotra G., Petrelli M., Sacco G., 2021. Shallow conduit

dynamics fuel the unexpected paroxysms of Stromboli volcano during the summer 2019. Scientific Reports 11, 266. https://doi.org/10.1038/s41598-020-79558-7.

Vona A., Romano C., Dingwell D.B., Giordano D., 2011. The rheology of crystal-bearing basaltic magmas from Stromboli and Etna. Geochimica et Cosmochimica Acta 75, 3214-3236.

Wallace G.S. and Bergantz G.W., 2005. Reconciling heterogeneity in crystal zoning data: An application of shared characteristic diagrams at Chaos Crags, Lassen Volcanic Center, California. Contributions to Mineralogy and Petrology 149, 98-112.

Waters L.E., Andrews B.J., Lange R.A., 2015. Rapid crystallization of plagioclase phenocrysts in silicic melts during fluid-saturated ascent: phase equilibrium and decompression experiments. Journal of Petrology 56, 981-1006.

Zhang Y., 2008. Geochemical Kinetics, 656. Princeton University Press, New Jersey.

Zhang Y., Walker D., Lesher C.E., 1989. Diffusive crystal dissolution. Contribution to Mineralogy and Petrology 102, 492-513. https://doi.org/10.1007/BF00371090.

Zieg M.J. and Lofgren G.E., 2006. An experimental investigation of texture evolution during continuous cooling. Journal of Volcanology and Geothermal Research 154, 74-88.